AlGaAs Phased Array Laser for Optical Communications

N. W. Carlson

David Sarnoff Research Center
Princeton, NJ   08540

FINAL REPORT

NASA

Table of Contents

PAGE _II_ INTENTIONALLY BLANK

List of Illustrations

List of Illustrations (cont.)

List of Illustrations (cont.)

PREFACE

This report describes work performed at the David Sarnoff Research Center in the Optoelectronics Research Laboratory, M. Ettenberg, Director, under Contract No. NAS1-18525. R. A. Bartolini and D. B. Carlin were project supervisors, and D. B. Carlin and N. W. Carlson were project scientists. Other contributors to this research were G. A. Evans, J. K. Butler, J. C. Connolly, L. Carr, N. A. Dinkel, L. Elbaum, R. Farkas, D. B. Gilbert, M. G. Harvey, F. Z. Hawrylo, C. J. Kaiser, J. B. Kirk, S. K. Liew, P. Pelka, W. Reichert, D. Truxal.

SUMMARY

The objective of this program has been to develop a monolithic AlGaAs phased array of semiconductor diode lasers suitable for optical communications. During this program, a number of diode laser array designs were investigated in an effort to develop the technology necessary to demonstrate a high-power coherent diode AlGaAs laser array for application as a source in free-space optical communications systems. These array structures include the channeled-substrate-planar (CSP) diode laser array, the ridge-guided diode laser array, and the grating-surface-emitting (GSE) diode laser array.

This array technology has been directed towards development of devices with modulation rate capabilities in the 0.3 to 4 Gbit/sec range, high power outputs in the 0.5-5 W cw range, single lobed diffraction limited far-field beam (stable under modulation), and single spectral mode operation with minimal wavelength chirp under modulation conditions. Our basic approach in this program was to investigate laser array structures that incorporate a grating structure in the form of a distributed Bragg reflector (DBR) or a distributed feedback laser (DFB). This was necessary to satisfy the wavelength stability requirement. To meet the far-field requirement, we initially investigated optimizing edge emitting laser array structures based on channeled-planar-substrate (CSP) and ridge-guide elements, laterally coupled both by evanescent waves and Y-guiding. None of these device structures ever demonstrated single-lobe far-field outputs at cw power outputs even close to the minimum goal level of 500 mW. Based on these results, it became clear that edge-emitting phased arrays would not satisfy the goals of this program.

Therefore, a new approach, based on the grating-surface-emitting (GSE) laser array was adopted about six months into the program. At the present time, grating-surface-emitting laser technology offers the greatest potential for achieving the goals of this program. Under this program, progress was made in extending the grating-surface-emitting laser technology to demonstrate a diode laser array suitable for optical communications systems. We discovered that the full power output of these arrays can be switched on and off by varying the current to only one gain section in the array. Modulation of the GSE array output by high speed-switching between stable laser array operation and no laser oscillation by the array offers a promising approach for meeting the modal stability

requirements in amplitude-shift-key (ASK) modulation schemes. Also, we have improved our understanding of the critical design issues that relate to single spatial and spectral mode operation under high rates of modulation. Based on this understanding, several new designs of GSE laser arrays were proposed.

Section I

INTRODUCTION

Diode lasers are very attractive for applications in coherent optical systems, such as free-space communication links, acousto-optic spectrum analyzers, optical recorders, laser radars, and optical computers. These applications often require a coherent source that operates in a single spectral and spatial mode, produces an output power of more than 500 mW cw, and emits a low-divergence single-lobed beam of light.

Individual diode laser emitters are limited to about 100 mW cw power output for reliable operation in coherent diffraction-limited beams. Such output levels are insufficient for the closure of many of the high-data rate, low bit-error-rate space communications links envisioned for future NASA missions. Coherent coupling of multiple emitters in phase-locked arrays, however, offers the promise of greatly multiplied power and has been an active area of research throughout the world during the 1980's.

This report will describe the research and development of coherent diode laser arrays. In this case, coherent array refers to both the temporal and spatial coherence properties of the array. For a communications source, it is necessary that the diode laser first have a high degree of temporal coherence as evidenced by single frequency operation with sufficiently narrow linewidth. In addition, the laser source must also have a high degree of spatial coherence over the emitting aperture in order to produce a high quality output beam. The topics presented are: 1) theory and modeling of laser arrays, 2) design of laser arrays, 3) wafer growth and processing, 4) grating-surface-emitting laser arrays, and 5) switching and modulation experiments on grating-surface-emitting (GSE) laser arrays, and 6) improved designs of GSE lasers for application as optical transmitters.

Section II

THEORY AND MODELING OF LASER ARRAYS

The theory of laser arrays involves finding the solutions for Maxwell's equations for the particular array structure in question. These solutions will give the mode amplitudes (near fields) of the array structure, as well as the operating wavelength of each mode and the modal gain. Solving Maxwell's equations for a laser array is a very complicated process, especially if effects, such as gain saturation, carrier diffusion, and thermal contributions are included. However, the salient properties of laser array modes can be understood by using models that neglect the aforementioned effects.[1,2] These models approximate the dielectric properties of laser array structures by what they would be in the absence of injected carriers and saturation effects, (i.e., cold cavity approximation). The two modeling approaches of this type that were used on this program were the coupled-mode theory[1] and a numerical solution of the two-dimensional array waveguide structure based on the effective index approximation (MODEIG).[2]

A. COUPLED-MODE ANALYSIS OF LASER ARRAYS

The coupled-mode formalism is well known in the field of integrated optics for analyzing periodic waveguide structures.[3,4] Since laser arrays are active periodic waveguides, they can be modeled using coupled-mode formalism.[1,5] The basic assumption of the coupled-mode theory is that the lateral modes of a laser array can be expressed as a linear combination of all the modes (both guided and radiation) of the individual lasers that comprise the array. In general, this is quite complicated. The calculation can be simplified if the array is made up of identical laser sections that only support a single transverse guided-mode and the geometry of the array waveguide sections is such that coupling between array elements is well approximated by nearest-neighbor interactions. In this situation, Maxwell's equation for the array reduces to a set of first order coupled differential equations for the amplitude of the array modes. These equations can be easily solved using matrix techniques.[1,5] The electric field (array mode amplitude) ,$E_p(x)$, corresponding to the pth lateral array mode is given by,

$$E_p(x) = E_0 \sum_{n=1}^{N} \sin\left[\frac{np\pi}{N+1}\right] \phi_n(x)$$

where N is the total number of elements in the array, p=(1,... ,N) is the array mode index, and $\phi_n(x)$ is the lateral mode profile of the nth array element. Figure 1 shows the normalized near-field amplitudes for the modes of a ten-element array.[1] The corresponding far-field patterns due only to the array amplitudes are shown in Fig. 2 (the contribution of $\phi_n(x)$ to the far field has been omitted). Each mode corresponds to a unique phase relationship between the array elements, and only the p=1 mode (in-phase) produces a far-field pattern with a dominant on-axis single lobe. The array mode that will experience laser oscillation will have the lowest threshold gain (lowest loss). Coupled-mode theory gives the modal threshold gain as,

$$G_p^{th} = G_0^{th} + 2 \, Re(\kappa) \, \cos\left[\frac{p\pi}{N+1}\right]$$

where G_p^{th} is the threshold gain of array mode p, G_0^{th} is the threshold gain of a single array element isolated from the array, and $Re(\kappa)$ is the real part of the nearest-neighbor coupling coefficient. $Re(\kappa)$ is determined by the lateral variation of the loss (imaginary part of the dielectric function) for the array structure. For structures with little or no lateral loss variation, such as purely index-guided arrays, there is no gain discrimination between different array modes. Such an array will oscillate in many lateral modes producing an output beam that has a very low spatial coherence. Therefore, it is critical to develop an array structure with sufficient lateral loss variation to obtain stable single array mode operation. Examples of array structures that fall in to this category are the channelled-substrate-planar array and anti-guided arrays.[6-8]

The coupled-mode theory is useful for calculating the threshold properties of arrays of lasers where the coupling is sufficiently weak that the lateral field of each array element is essentially unperturbed by the presence of the array structure. It illustrates the important connection between the array structure and array mode discrimination. However, it is not a good approximation for array structures that are strongly coupled. In this situation, it is better to use a numerical approach based on the effective index-approximation.
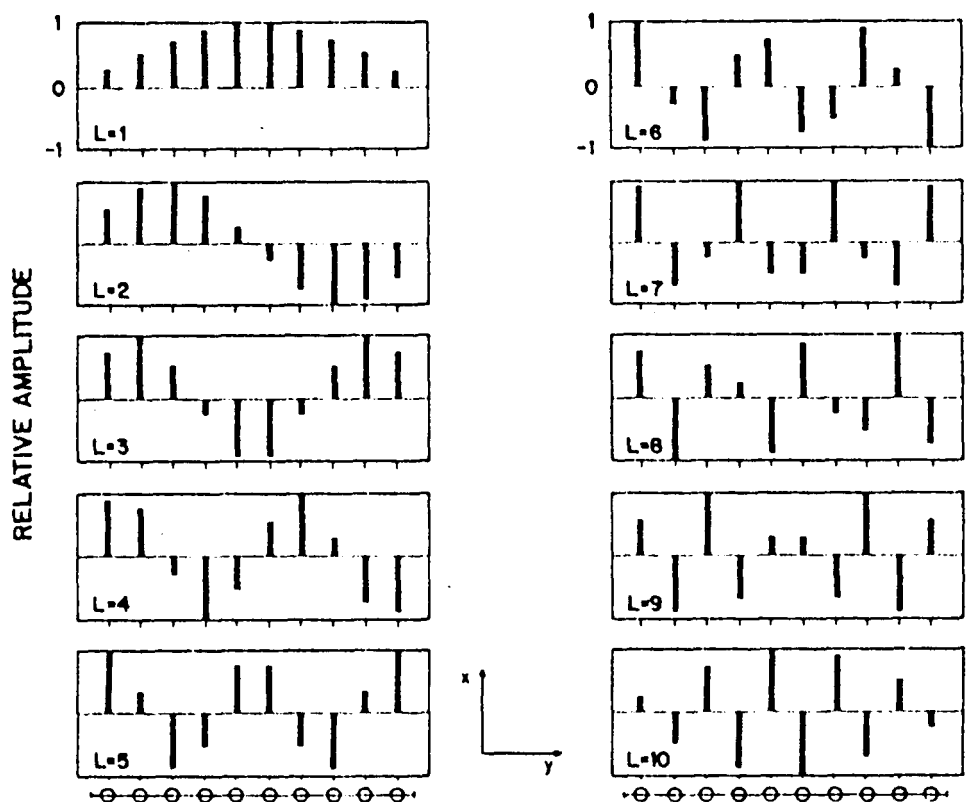
Figure 1. The normalized amplitudes of the modes of a ten-element
array are shown. Amplitudes that extend below the center
line indicate a 180° phase relative to those above the center
line.
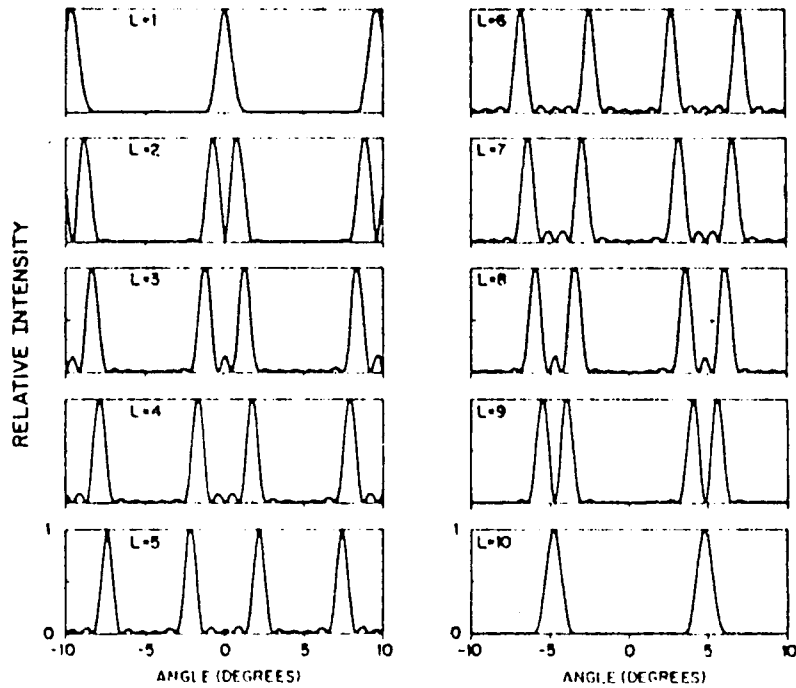
Figure 2. The far-field patterns corresponding to the modes of a ten-element array are shown. The spacing between array elements was 5 μm.

B. NUMERICAL ANALYSIS OF ARRAY STRUCTURES: LINEAR THEORY

It is almost always possible (at least in principle) to solve Maxwell's equations using computer models based on numerical methods. In fact, the numerical techniques necessary for treating laser arrays are exactly those used in integrated optics for treating coupled multi-layered waveguides with complex dielectric properties.[9,10] These techniques are based on the effective index method, wherein each mode of a multi-layered waveguide is specified by a single complex modal propagation constant. For a specific wavelength the effective index of the mode and the modal loss are easily obtained from the complex modal propagation constant. The modal properties of the array at threshold can be well approximated by treating the array as a passive waveguide structure. Unlike the coupled mode approach, this is not a perturbative treatment, so strongly coupled arrays of lasers can be modeled, as well as non-uniform structures.

Since the laser array problem is a two-dimensional waveguide problem, it is necessary to apply the effective index method twice. First the modal effective

6

indices and losses for the transverse fundamental modes are calculated for the different structures that occur along the lateral direction (see Fig. 3a). These different waveguide structures are then approximated as bulk layers with the dielectric properties given by the transverse modal effective indices and losses, as shown in Fig. 3b. The modes of this lateral stack, which correspond to the array modes, are then calculated using the effective index method. For an N-element array, a total of N guided modes are found, as was the case in the coupled mode theory. Using the effective index approximation, as described above, for laser arrays is valid when the transverse structures that comprise the array support only one guided mode or the losses of the other guided modes are much greater than that of fundamental mode.

(a)

(b)
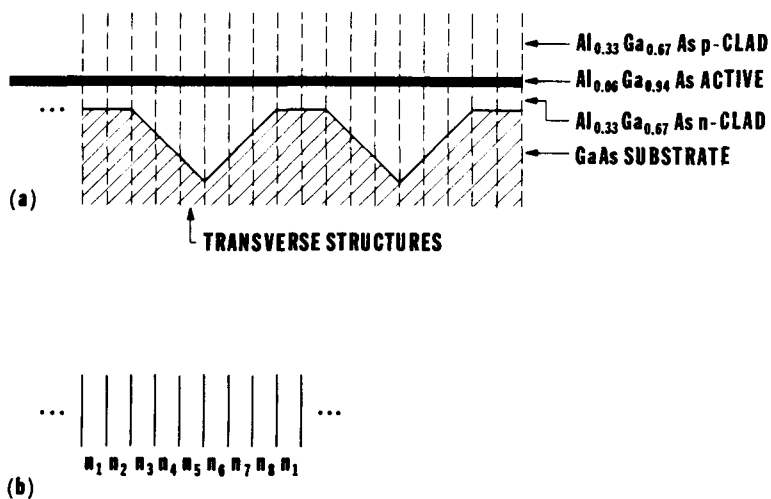
Figure 3. a) A schematic diagram of the lateral geometry of a laser array and epilayer composition. The transverse dotted lines indicate the finite regions over which the effective index-method is applied. b) A schematic diagram of the reduced array structure after the effective index method has been used to calculate the effective dielectric constant due to the transverse structure.

Using a computer model, based on this numerical approach, has proven to be a useful starting point for designing and optimizing laser structures. The computer model that is used at David Sarnoff Research Center for analyzing array structures is called MODEIG.[2] With this computer model it is possible to calculate the properties of an array mode as a function of layer thicknesses or composition (dielectric properties). This feature of the computer model is very useful for optimizing the structural parameters of the array with respect to desired modal characteristics. This procedure was used in designing the channelled-substrate-planar arrays (discussed in Section III) that were fabricated for this program.

Although MODEIG is useful for determining the threshold properties of arrays, it cannot be used for calculating array characteristics above threshold, such as the power vs current curve. In order to model these properties, a nonlinear model that incorporates gain saturation and current diffusion is needed.[11]

C.   ARRAY DESIGN APPROACHES

The goal of any phased array design is to produce a device that operates in a pure 0° in-phase lateral mode over a broad range of operating conditions. In most situations, phased arrays oscillate in several array modes with a dominant contribution from the 180° out-of-phase mode. This occurs because the region between the laser sections of the array usually have a higher loss than the laser channels themselves. As is the case with any laser, the laser array preferentially oscillates in the mode with the lowest loss. For most arrays, the 180° mode will usually have less field in the lossy regions between channels than the 0° in-phase mode, as shown by the schematic diagram in Fig. 4.

Insufficient gain discrimination between lateral modes will cause the array to oscillate in several spatial modes. Array mode discrimination is determined by the lateral spatial variation in the imaginary (loss/gain) part of the dielectric function. To achieve stable single array mode operation over a wide range of operating conditions, the lateral variation in the complex dielectric function should be strong enough so that it is relatively insensitive to modification of the gain medium by changes in the carrier injection level and interactions with the optical field.

8

**NEAR FIELD AMPLITUDE
PROFILES**

**FAR FIELD INTENSITY
PROFILES**

0°-PHASE-SHIFT
ARRAY OPERATION

180°-PHASE-SHIFT
ARRAY OPERATION
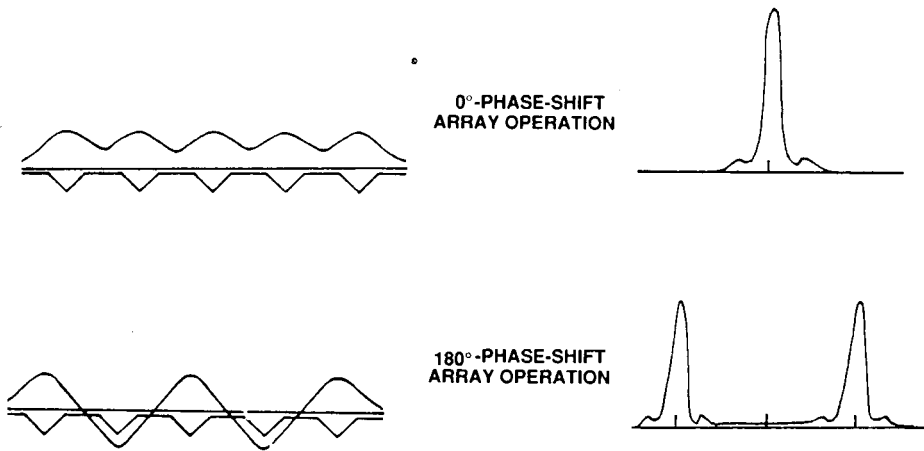
Figure 4. The near field and far-field patterns of 0° phase-shift and 180° phase-shift operation.

9

Section III

CHANNELLED-SUBSTRATE-PLANAR DIODE LASER ARRAYS

Under cw operation, the channelled-substrate-planar (CSP) single-element diode laser has demonstrated single frequency operation in a single spatial fundamental mode with power outputs up to almost 100 mW.[12] Results obtained on CSP diode laser arrays (structure shown in Fig. 5) for the Coherent High-Power Phase Array Laser Semiconductor (CHIPPALS) program demonstrated eight-element arrays with high spatial coherence that operated in a pure 180° phase mode up to about 50 mW cw power output.[13] Although it is the 0° phase mode and not the 180° mode that is desired, it was decided to try to develop such a CSP array that would operate at cw power outputs up to 1 W. The reason for this was that at the start of the program the CSP arrays were the only arrays reported (reference 6 and 7) that demonstrated high spatial coherence over a wide range of operating conditions. An external phase shift plate arrangement, shown in Fig. 6, would then be used to obtain the 0° phase shift mode. In order to develop a higher power CSP array, it was necessary to increase the number of array elements. In the first design, it was decided to fabricate 8-, 12-, and 20-element CSP diode laser arrays. The reason for this choice of element numbers was to investigate how many elements could be laterally coupled and still maintain good coherence; it has already been demonstrated that eight-element arrays could be highly coherent. Below is a description of the growth processing, followed by a description of the test results.
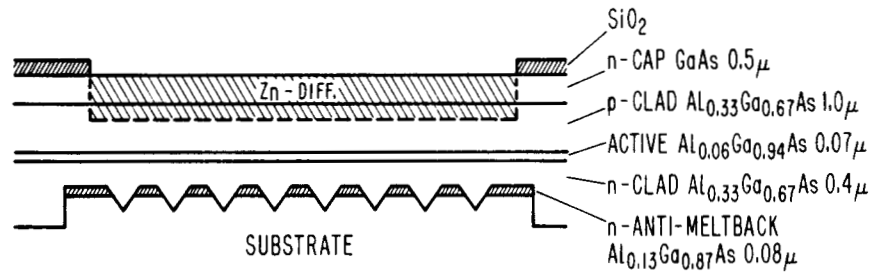
Figure 5. Schematic diagram of CSP laser array structure that was grown. The photographs show stained cross-sections of the array structures that were obtained under different growth conditions.
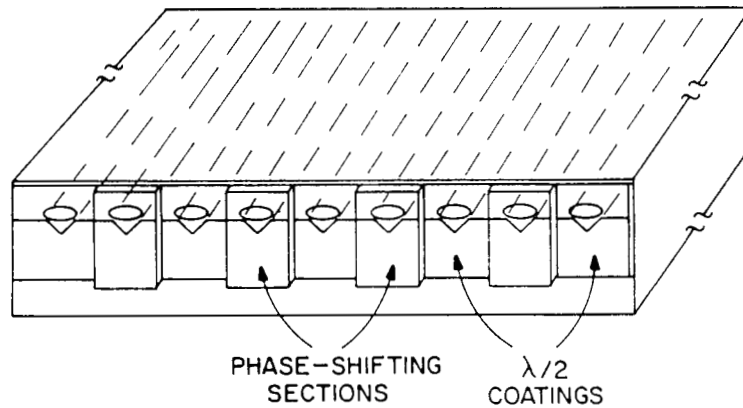
Figure 6. A schematic diagram showing a phase shift correction method for converting the 180° phase mode to the 0° phase mode. The phase shift plate consists of alternating half-wave coatings on the facet of the array.

A. WAFER GROWTH AND PROCESSING OF CSP DIODE LASER ARRAYS

The wafer growth for CSP laser arrays consists of two steps, since the channels must be etched. In the first step, metal-organic chemical vapor deposition (MOCVD) is used to grow a GaAs buffer layer (about 4 μm thick) over the GaAs substrate. An $Al_xGa_{1-x}As$ anti-meltback layer (x= 0.1 - 0.15 and thicknesses ranged from 0.1 μm to 0.9 μm) was then grown over the GaAs buffer layer by MOCVD. This layer was found to be necessary to preserve the desired shape of the CSP channel after LPE regrowth as discussed below.

Before the epilayers that comprise the diode laser are grown, the channelled mesa structures are chemically etched to a depth of anywhere from 1 μm to 2 μm. These channelled mesas provide the lateral control, confine the optical mode to those channels within the mesa, and reduce meltback of the channels during regrowth. In this process, the first step is to spin photoresist over the entire wafer. Next, the mask with the appropriate channelled mesa geometry is used to expose the photoresist only in the regions of the channels and outside the mesas. After the exposed photoresist is removed, the channelled mesas are chemically etched into the wafer through the openings in the photoresist. Upon completion of the etch, the remaining photoresist is removed from the wafer and the wafer is prepared for the second growth step.

The second and final growth step of the laser epilayers is done by liquid phase epitaxy (LPE). Figure 5 shows a schematic diagram along with stained cross-sections of two completed laser arrays. The array cross-section on the left has an anti-meltback layer whereas the one on the right does not. As a result, the channels in the array on the right show significantly more meltback than do the channels of the array on the left. Since LPE growth is an equilibrium process, the shoulders between the channels can dissolve into the liquid melt during the growth of the n-clad layer over the channels. For this reason an AlGaAs layer, referred to as the anti-meltback layer above, is grown over the entire wafer to reduce this meltback. In addition, the channels are etched into the tops of mesas (shown in Fig. 5) that are etched into the GaAs buffer layer. This also helps reduce the meltback.

After the LPE regrowth, SiO_2 is deposited over the entire wafer and then removed only directly above the channelled mesas (see schematic diagram in Fig. 5). Then, a zinc-diffusion is done through these openings in the SiO_2 to provide confinement of the injected current. This is followed by a Ti/Pt/Au

metallization on the p-side and a Au/Ge metallization on the n-side. After the wafer is cleaved into bars, the bars are coated with a 90% reflecting dielectric stack on the back facet and a 10% dielectric reflecting stack on the front facet. The bars are then diced into chips that contain single arrays, and these arrays are soldered onto mounts. Once mounted, the arrays are ready for testing.

B. PERFORMANCE CHARACTERISTICS OF CSP LASER ARRAYS

The basic optoelectronic properties of the arrays were measured using an automated diode laser tester. This automated test facility measures the power current curve, voltage current curve, parallel and perpendicular far-field patterns, and the spectral output. These characteristics can be measured for both cw and pulsed operation. After this first round of testing, the devices with the best characteristics are selected for further testing. Since hundreds of lasers are obtained from a single wafer, it is necessary to select only those arrays with acceptable performance characteristics. More detailed (and time consuming) measurements, such as near-field intensity distribution, near-field phase and spatial coherence, wavefront quality, and modulation characteristics, are then done on these selected devices.

C. BASIC OPTOELECTRONIC PROPERTIES OF CSP LASER ARRAYS

The CSP laser arrays did not perform as expected. Even the eight-element arrays did not operate in a highly coherent single array mode as had been previously observed. Figure 7 shows the power (from one facet) current curves of 8-, 12-, and 20-element CSP arrays (with uncoated facets) that were operated under pulsed conditions. These 8-, 12-, and 20- element arrays had channels that were 4 μm wide on 5 μm centers. The shoulder between adjacent channels was 1 μm wide. As expected the 20-element arrays had the largest power output (500 mW per facet). However, all arrays operated multi-spatial mode and did not have good spatial coherence as evidenced by the far-field pattern. In Fig. 8, both the near-field and far-field patterns are shown for a 20-element CSP array. The far-field pattern is double lobed as expected, and the widths of the lobes broadened as the power output was increased. This broadening is an indication of multi-spatial mode operation. The near-field pattern also supports this interpretation. Note that the intensity between the channels does not go almost to zero as it should for a pure 180° phase mode operation.[1,8]

LJ-159 UNCOATED

Peak Power (mW)

500

400

300

200

100

0

0.0 0.4 0.8 1.2 1.6 2.0

Current (A)

o #1 8 Element
▲ #2 8 Element
• #3 12 Element
△ #4 20 Element
■ #5 20 Element
□ #6 20 Element
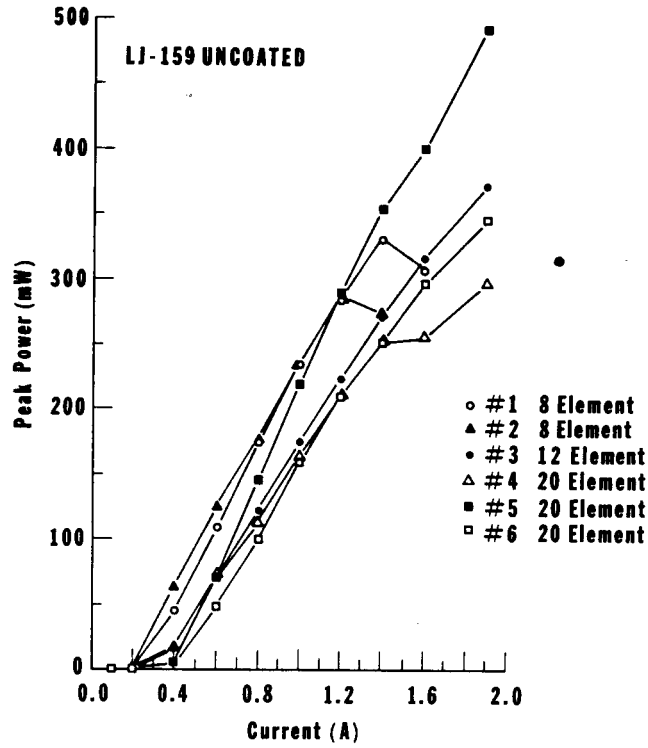
Figure 7. The power vs current curves for CSP laser arrays with 8, 12, and 20 elements.

Near Field Intensity

5μm

350mW

0 25 50 75 100 125

Near Field Position (μm)

Far Field Intensity

— 353mW
····· 219mW
--- 71mW

Power	ΔΘ$_{FWHM}$
71mW	1.5°
219mW	2.5°
353mW	4°

-10 0 10

Far Field Angle (deg.)
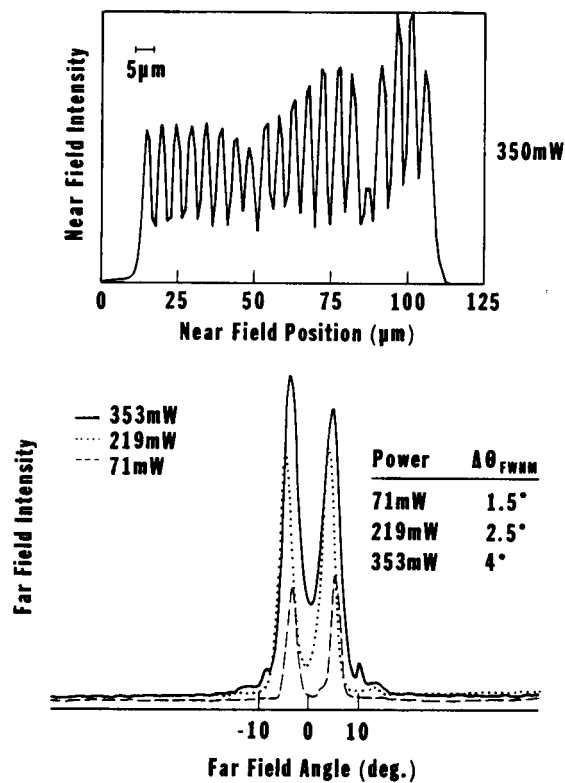
Figure 8. The near and far-field outputs of a 20-element CSP laser array.

15

The reason for the poor performance of these CSP arrays is due to the nonuniformities in the layer thicknesses across the wafer resulting from the LPE growth process. MOCVD grown wafers are known to have better uniformity of layer thicknesse, however, the techniques to do MOCVD growth over channeled structures were not developed anywhere at the start of this program. Because of the time and resources involved, no attempt was made to develop these techniques on this program. It was difficult to fabricate diode laser arrays reproducibly using LPE. Modeling results of arrays have shown that structural nonuniformities, of the type that can occur in LPE,[11] can cause instabilities and multiple-lateral array mode operation. For this reason, it was decided that LPE should no longer be used to fabricate the CSP arrays. A more uniform growth process, such as MOCVD should be used. However, the techniques for growing over channelled structures with MOCVD were not developed. For these reasons (and others described below), a decision was made to abandon the CSP edge-emitting laser arrays and instead use an approach based on the grating-surface-emitting (GSE) diode laser array.

Section IV

GRATING SURFACE EMITTING LASER ARRAYS

During the course of this program, rapid developments in injection-coupled grating surface emitting (GSE) laser array technology[14-17] on the Phase Integrated Laser Optical Technology (PILOT) program caused us to reconsider the approach for the final design. Linear GSE arrays had demonstrated 400 mW peak power outputs from just the p-side.[14] Since these arrays were operated p-side up, about three times as much power was radiated into the n-side GaAs substrate, where it was absorbed. Hence, this array probably had a total potential emission in excess of 1W. Shortly after this result, the first two-dimensional GSE laser array was demonstrated. This device operated at power outputs up to 1W (p-side up testing under pulsed conditions). At power outputs of 200 mW, a far-field output consisting of a dominant single lobe with an angular divergence of 1° x 0.01° was obtained by optimizing the currents to each gain section. The spectral output of these first devices typically had bandwidths 3 Å at 1 W power output[16] and 0.25 Å near threshold.[17] In some cases, this is too broad for the goals of this program. However, it is still much narrower than the spectral width of high-power edge-emitting arrays when operated under similar pulsed conditions.

These results were more encouraging than those obtained thus far from the edge-emitters. Furthermore, GSE lasers could be superior to edge-emitting arrays for the following reasons:

1) Larger emitting area gives a narrow far field divergence

2) Stable spectral output due to grating

3) Grating emitters are very robust compared to facets; catastrophic facet damage is not a problem

4) Spatial mode selectivity is possible by tuning currents to the independent gain sections

By growing wafers on transparent substrates, it is possible to utilize the light that is coupled out of both the p-side and the n-side. This is accomplished by high reflecting coating the p-side of the wafer over the DBR sections and anti-reflection coating the n-side so that most of the light is emitted through the transparent n-substrate. Such a device would also be mounted p-side down so that the active areas would be closer to the heatsink making cw operation possible. The modulation capabilities of GSE laser arrays had not yet been investigated

17

experimentally. However, the GSE array design is very similar to multiple gain section edge-emitting diode lasers, which had already demonstrated multi-Gbit modulation rate capabilities.[18-20] It was, therefore, decided to follow an approach based on GSE laser array technology. For the reasons mentioned above, this technology offers the greatest potential for developing a monolithic diode laser source suitable for optical communications systems.

A.   PRINCIPLES OF GSE LASER ARRAY OPERATION

The basic design of a monolithic linear GSE laser array is shown in Fig. 9. It consists of electrically independent gain sections that are injection coupled through second-order distributed-Bragg-reflector (DBR) waveguides. The structure is monolithic because the gain sections and DBR sections are fabricated along a common planar waveguide. So the active-waveguide layer in the gain sections also acts as a passive-waveguide layer in the DBR sections. Because the DBR section is not injected with current, the presence of an unpumped active layer can introduce a large loss into the GSE laser cavity. This problem is avoided by using a single- or multi-quantum well active layer structure. Such active layer structures can be designed to have absorption losses that saturate to less than 10 cm^{-1} at optical powers of only several mW. At these low loss levels, sufficient light is transmitted through a DBR section of several hundred microns in length to injection-couple the gain sections. Since the DBR sections contain a second-order grating, they also provide the optical feedback to the gain sections necessary to sustain laser operation and act as output couplers. The ability to individually address each gain section of the GSE array makes it possible to adjust the current to different gain sections so that single longitudinal mode operation is obtained.[14-17] This adjustment can also change the relative phases of the light emitted from different DBR sections. Therefore it may be necessary to add a phase-shift filter on the DBR output sections to obtain 0° in phase emission. If each gain section along the longitudinal direction (injection-coupled direction) of the array were to consist of a group of laterally coupled lasers, then a two-dimensional GSE laser array would be obtained.[16,17]
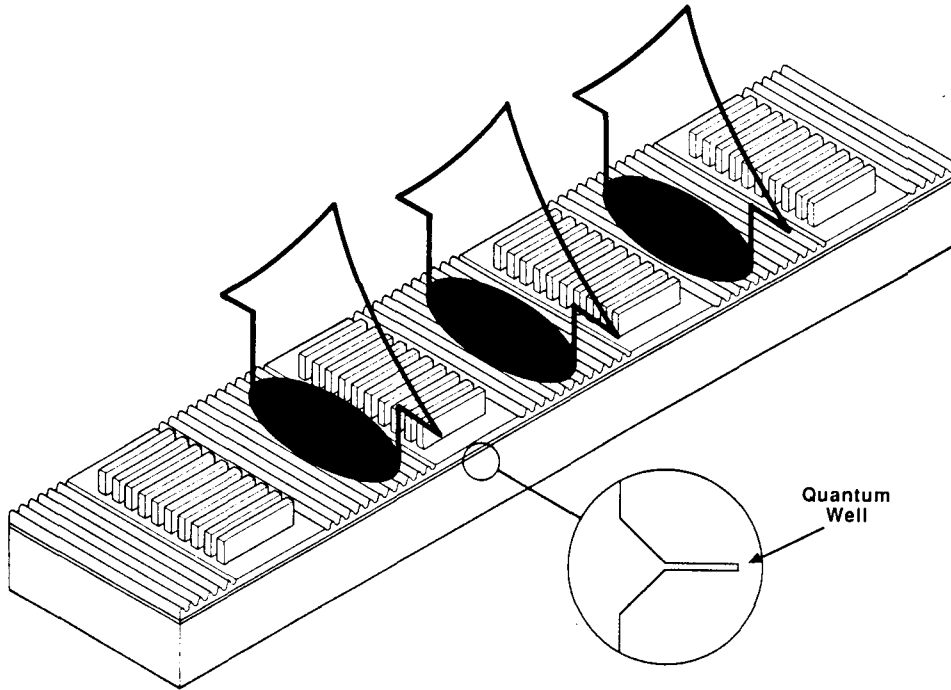
Figure 9. A diagram of a two-dimensional GSE laser array. The large
arrows represent the output coupled light, and the inset shows
the structure of the GRINSCH-quantum well active
waveguide layer.

A GSE array that operates at a single frequency (high temporal coherence)
can be modeled as a single long laser section in which the feedback and output
coupling are distributed at discrete locations along the laser cavity in the form of
the DBR sections. The important parameters that need to be considered for
optimizing the GSE array are the DBR section reflectivity, r, the DBR
transmissivity, t, and the losses due to both the surface-emitted light and
absorption/scattering in the common waveguide. Recently, a network theory was
developed for modeling the threshold characteristics of two-dimensional laser
arrays with arbitrary coupling schemes.[21] Since this is a general theory, it can
also be used to model the threshold properties of GSE arrays, such as threshold
gain and differential quantum efficiency. For a uniform linear array of injection-
coupled GSE lasers the threshold gain per unit length, $G_{th}(N)$, of an injection
coupled array with N injection-coupled gain sections is given by,[22]

$$G_{th}(N) = \alpha + \frac{1}{L} \ln \left[\frac{1}{\sqrt{1-a^2}} \right] + \frac{1}{NL} \ln \sqrt{\frac{|t|^2}{|r|^2} + 1}$$

where L is the length of a gain section, a is the optical loss per unit length in a gain section and $a^2 = 1 - |t|^2 + |r|^2$ is the fractional power loss in a DBR section due to all sources (i.e., absorption losses and grating surface emission). The second term in the above equation represents the loss per unit length in the DBR sections and the third term represents the end losses when the array is terminated by uniform regions with unpumped gain sections. The above equation is applicable to two-dimensional GSE laser arrays.[21,22] As the number of gain sections is increased, the end loss term decreases so the threshold current per gain section will decrease as the number of gain sections in the array. As the number of gain sections increases, the threshold gain approaches a constant given by,

$$G_{th}(\infty) = \alpha + \frac{1}{L} ln \left[\frac{1}{\sqrt{1 - a^2}} \right]$$

The differential quantum efficiency, $\eta_Q(N)$, is the ratio of the change in optical power output to the corresponding change in electrical power input to the laser. For a GSE array with N injection-coupled elements it is given by,

$$\eta_Q(N) = \eta_0 S \left\{ \frac{1}{L G_{th}(N)} ln \left[\frac{1}{\sqrt{1 - a^2}} \right] \right\} \left[1 - \frac{1}{N L G_{th}(\infty)} ln \sqrt{\frac{|t|^2}{|r|^2} + 1} \right]$$

where η_0 is the internal quantum efficiency of the gain sections, and S is the ratio of useable surface-emitted power emitted from a DBR section to the total power loss in a DBR section. Each of the bracketed factors in the above equation has an understandable physical basis. The factor in the pair of braces is the ratio of the total power lost in the DBR sections to the stimulated power. This is multiplied by S to get the fraction of useable surface-emitted power. The term in square brackets accounts for the power lost at the ends of the array when it is terminated by uniform regions of unpumped gain sections. As the number of gain sections is increased (array size increased) this factor approaches unity, and the end losses become negligible.

In Fig. 10 both the threshold gain and quantum efficiency have been plotted as a function of N over the range of N=1 to 10. The array parameters used in Fig. 10 correspond to those of typical GSE arrays so far reported with GRINSCH-SQW structures for gain sections. By minimizing, a, the optical losses in the gain

sections (a @ 5 cm⁻¹ is the lowest loss reported for GRINSCH-SQW material) and maximizing, S, the fraction of the power lost in the DBR sections that goes into usable surface-emitted power, the threshold characteristics can be optimized, as shown in Fig. 11. In Fig. 10, S = 0.3 corresponds to the case when only the surface-emitted light from the p-side is usable. This is the situation for devices grown on GaAs substrates. Since the substrate is absorbing at the laser wavelength, the grating-emitted light from the n-side is not useable. However, by growing wafers on transparent AlGaAs substrates it is possible to make use of the grating-emitted light from both the p-side and the n-side, as discussed above. In this case, it should be possible to increase S to about 0.8. For the optimized device, $\eta_Q(N)$ is calculated to be about 75%, which is comparable to the best edge-emitting lasers. The reduction in gain for a ten-element array from about 65 cm⁻¹ to about 25 cm⁻¹, should correspond to almost a factor of "three" reduction in the threshold current density for GRINSCH-SQW gain sections.[22] The network model of injection-coupled GSE laser arrays shows that an optimized GSE array has threshold characteristics that are comparable to those of the best edge-emitting lasers.

(Losses Estimated From Experiment)
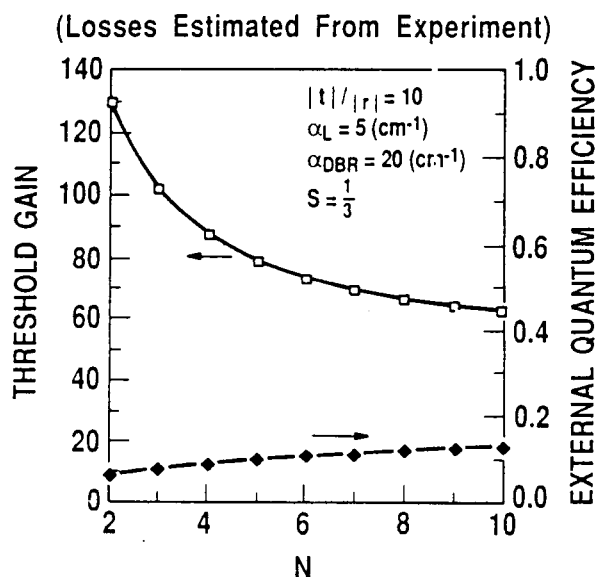
Figure 10.   The calculated threshold gain and external quantum
             efficiency are shown as a function of N, the number of gain
             sections in the array, for present GSE laser arrays
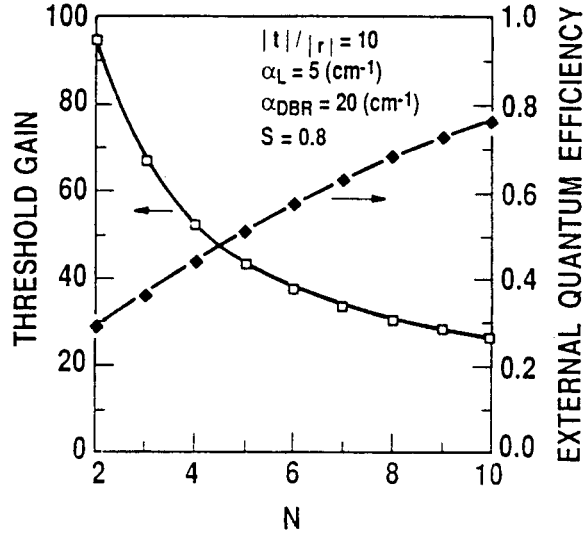
Figure 11.   The calculated threshold gain and external quantum efficiency are shown as a function of N, the number of gain sections in the array, for an optimized GSE laser array.

B.   GROWTH AND PROCESSING OF GSE LASER ARRAYS

Wafers from which the GSE laser arrays for this program were fabricated were all grown by metal-organic chemical vapor deposition (MOCVD).   This structure, shown in Fig. 12, consisted of a graded index separate confinement heterostructure (GRINSCH) with a single quantum well (SQW).   After the growth, a Zn/In diffusion was done over the entire surface (p-side) of the wafer, followed by an evaporation of Ti/Pt/Au over the complete wafer.   In the next step, the first level mask was used to define the gain sections in photoresist.   Two types of gain sections were used for the two-dimensional GSE arrays.   One design, shown in Fig. 13,   consisted of ten evanescently coupled ridge-guided lasers.   The ridge guides were 3 μm wide and on 6 μm centers.   The other type of gain section consisted of ten Y-coupled ridge-guided lasers.   In this design, the ridge guides were 2 μm wide and separated by 5 μm in the straight sections of the Y-guides. Areas of the metallization not covered by the photoresist were then removed by ion-beam etching.   The cap layer and a portion of the p-clad were also removed (from those areas not covered by photoresist) by ion-beam etching.   The evanescently coupled ridge guides or Y-coupled ridge guides are those remaining areas of cap and p-clad that were protected by the photoresist.   The thickness of the p-clad that is left is usually between 1000 μm and 2400 μm from the top of the underlying GRINSCH structure, depending on the width of the underlying

GRINSCH structure. Since the grating is fabricated in the remaining p-clad, it is important that the p-clad be sufficiently thin so that the optical field interacts with the grating. Photoresist is then spun on the wafer followed by a holographic exposure using the 3511 Å of optical emission line an argon ion laser. The photoresist is then developed, forming the grating (with a period of about 2500 Å) in the photoresist. Using ion-beam etching, this photoresist grating is replicated into the p-clad of the wafer to a depth of about 600 - 1000 Å. After grating fabrication, a plasma deposition process was used to deposit a 3000 Å thick layer of Si_3N_4 over the entire wafer surface. A photolithographic technique was then used to remove the Si_3N_4 only on the tops of the 3 μm wide gain sections. Then the p-surface of the wafer was re-metallized with 500 Å of Ti and 1000 Å of Au using electron-beam evaporation. The contact pad areas were then defined as openings in a photoresist layer that was spun over the entire wafer. These openings correspond to the contact pad dimensions, which were 150 μm wide and the same length as the gain section, which was 150 μm long. The length of the DBR sections between gain sections was 300 μm. Gold contact pads were then plated (through the openings in the photoresist) up to a thickness of 1 μm. After the photoresist was removed, the thin layer of p-metal (500 Å of Ti and 1000 Å of Au) was removed by ion-beam etching to electrically isolate the gain sections. At this point, the wafer is thinned by lapping the GaAs substrate on n-side to a thickness of 4 mils. A Au/Ge/Ni/Au metallization is then deposited over the entire n-side of the wafer. This completes the processing of the wafer.

GRINSCH-SQW Active Layer

**Ridge-Guided
Gain Section**

3μm ← | ← 6μm →

p-Clad ~0.1μm
Active
n-Clad

Mole Fracture AlAs

100
80
60
40
20
0

Cap (0.2μm)

p-Clad
(1.2μm)

n-Clad
(1.2μm)

Quantum Well (50Å)

Graded
Regions
(0.4μm)

Substrate

4 x 10 GSE

300μm

150μm

2nd Order Grating

~2500Å Period   ⇧ al$_{in}$

l$_{in}$ →

rl$_{in}$ tl$_{in}$

p-Clad ~0.1μm
Guide Layer
n-Clad

2nd Order DBR Passive Waveguide Section
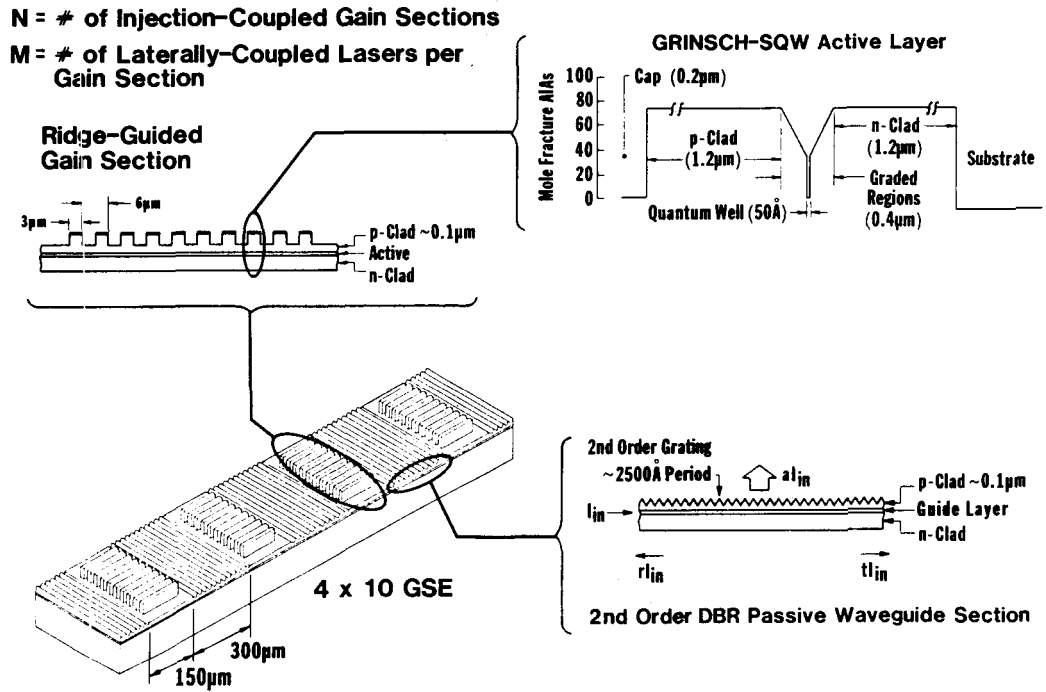
Figure 12. The composition and dimensions of the GRINSCH-SQW
structure that was used for GSE laser arrays.

4100Å

%Al

← T →

80

20

0

← 50Å →

p-CLAD

n-CLAD
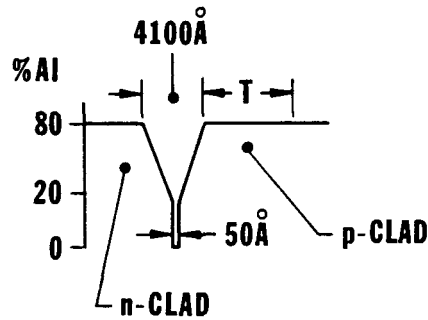
Figure 13. A schematic diagram of a monolithic two-dimensional GSE
diode laser array. The insets show the geometry of the
evanescently coupled ridge-guide lasers in the gain
sections, the structure of the GRINSCH-SQW
active/waveguide layer, and the DBR passive waveguide
structure.

C. PROBE TESTING AND P-DOWN MOUNTING OF GSE ARRAYS

After processing, all wafers are probe tested (0.1%-2% duty cycle pulsed operating conditions with 50-ns-long pulses) p-side up to identify the sections of the wafer that contain operating linear GSE arrays with suitable operating characteristics. The probe test station can drive arrays with as many as ten injection-coupled gain sections. Using the probe tester it is possible to measure the power vs current curve, near-field pattern, far-field pattern, and the spectral output. Examples of the near-field emission patterns of a two-dimensional GSE array under probe testing is shown in Fig. 14. The black pointed shapes are the current probes through which current is injected into the gain sections. Once the best GSE arrays have been identified on the wafer, the wafer is sawed into bars and the bars are mounted in a suitable package so that more comprehensive testing can be done.

D. 1 X 10 RIDGE-GUIDED GSE DISTRIBUTED-BRAGG-REFLECTOR LASER ARRAY

Since the design approach was to be a GSE laser array, experiments were planned that were aimed at fabricating a GSE laser array that would satisfy the program goals. To this end, the first surface-emitting device fabricated and characterized was a 1 x 10 ridge-guided GSE DBR laser array. The structure of this array is shown in Fig. 15. The reason this structure was selected was that it had only one gain section and one grating emitter. Therefore, the shape of the far-field pattern should be insensitive to changes in the driving current. Also, a single grating emitter gives an output beam with a smaller aspect ratio. The insets in Fig. 15 show a cross-section of the laterally coupled ridge-guides, a diagram of the structure and composition of the epilayers, and a side view of the DBR section. These 1 x 10 GSE arrays were obtained by cleaving from a wafer to get the appropriate facets. The facet on the gain section was high reflect.
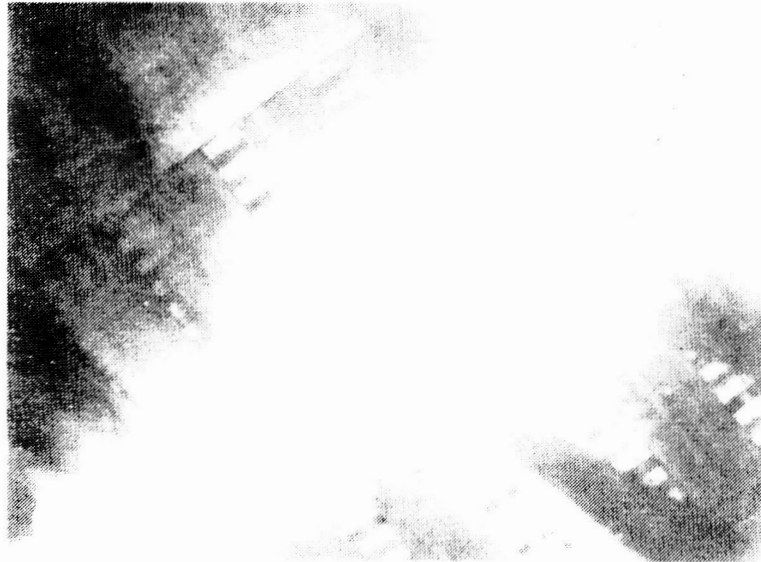
Above Threshold
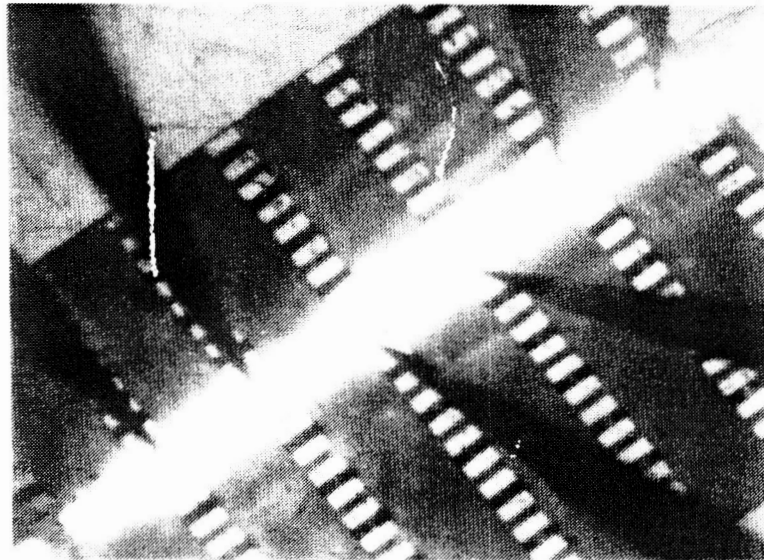
Below Threshold

Figure 14. Near fields of a 10 x 10 GSE array taken during probe testing. The near field is shown both above and below threshold.
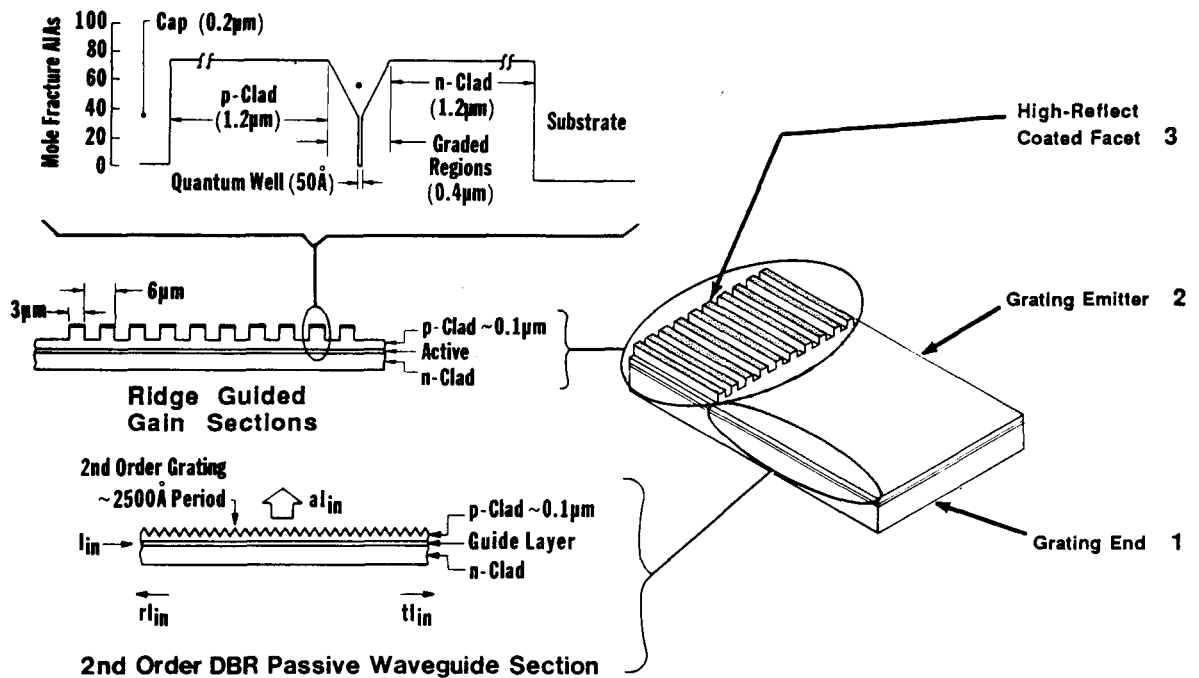
Figure 15. A schematic diagram of a 1 x 10 ridge-guided GSE diode laser
array. The insets show the geometry of the evanescently
coupled ridge-guide lasers in the gain sections, the structure
of the GRINSCH-SQW active/waveguide layer, and the DBR
passive waveguide structure.

Figure 16 shows the power vs current curve for the 1 x 10 GSE array
obtained under pulsed operating conditions (2% duty cycle, 50 ns pulse width).
The three curves correspond to the power from the facet at the end of the DBR
section (1), the surface of the DBR section (2), and the high reflect coated facet on
the gain section (3). About a factor of five more power is emitted from (1) the facet
at the end of the DBR section than is emitted from (2) the DBR surface. This
indicates that the coupling of the guided light to the grating in the DBR section is
weak. The spectral output of this array is shown in Fig. 17 for pulsed operation at
peak power outputs of 140 mW and 400 mW. This spectrum was measured using
the light that was emitted from (1) the facet at the end of the DBR section. At both
power outputs multimode operation is observed. It is likely that this was caused
by the weak grating in this structure. A weak grating is characterized by a low
reflectivity and higher transmissivity. Thus, the broadband feedback from facet
reflections will dominate over the frequency selective feedback due to the grating
and the laser will operate multimode. Another cause of the multimode operation
could be wavelength chirp due to pulsed operation of the device.

Other 1 x 10 GSE arrays identical in structure to that shown in Fig. 15 but with stronger grating coupling were also tested. The power vs current curve is shown in Fig. 18. Because most of the power output was emitted from the grating section, the grating coupling for this device was stronger than that which gave the data shown in Figs. 16 and 17. In this device most of the power was emitted from the surface of the DBR section, and very little was emitted from either of the facets. This array was also operated under pulsed conditions and only produced 100 mW. The reason for the relatively low power output of this device is not known. The spectral outputs under pulsed operation at peak power outputs of 20 mW and 90 mW are shown in Fig. 19. Both of these spectra show broadening. The resolution limit of the instrument used for the measurement was 1 Å. This is probably due to wavelength chirp caused by the pulsed operating conditions. Under dc operating conditions a narrower spectral output would be expected for a device with such a strong grating. Because these arrays were mounted junction-side (p-side) up, it was not possible to obtain cw operation due to the poor heatsinking.
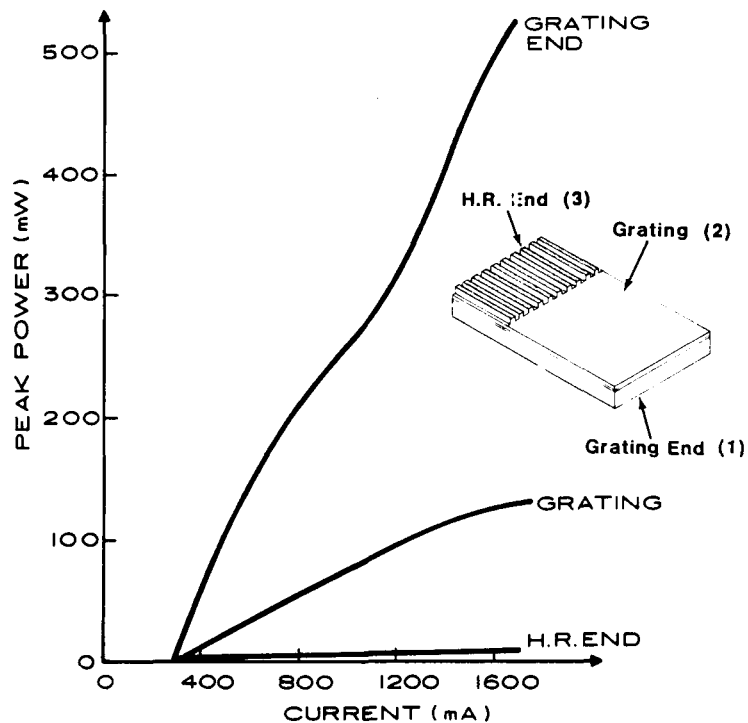
Figure 16. The power vs current characteristics for a 1 x 10 ridge-guided GSE laser array with a weak grating. The power output was measured from both facets, as well as the grating in the DBR section.
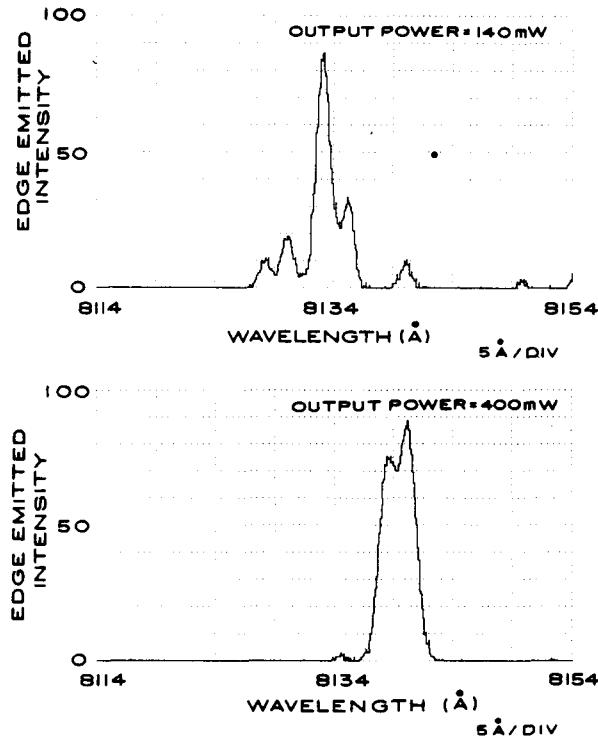
Figure 17. The spectral outputs of the 1 x 10 GSE laser array with a weak grating are shown at peak power outputs of 140 mW and 400 mW for pulsed operation with 2% duty cycle and 50-ns-wide pulses. Note that these spectra were obtained from (1) the grating end of the laser associated with the data in Fig. 16.
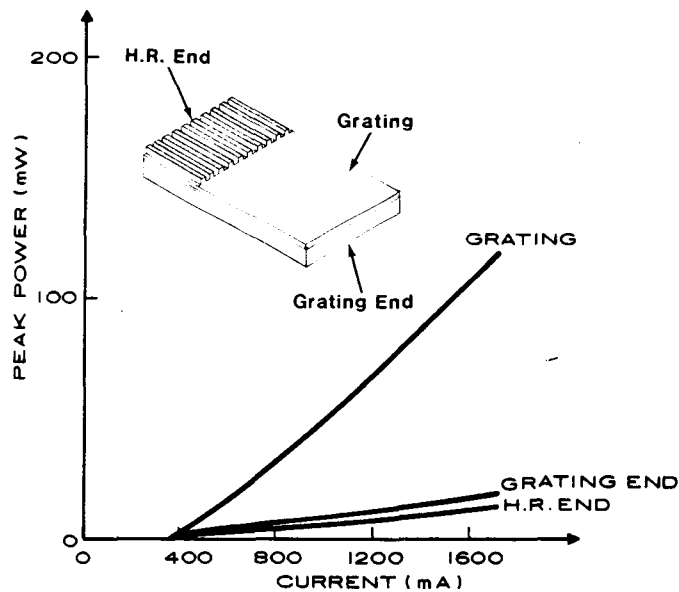
Figure 18. The power vs current characteristics for a 1 x 10 ridge-guided GSE laser array with a strong grating under pulsed operating conditions.
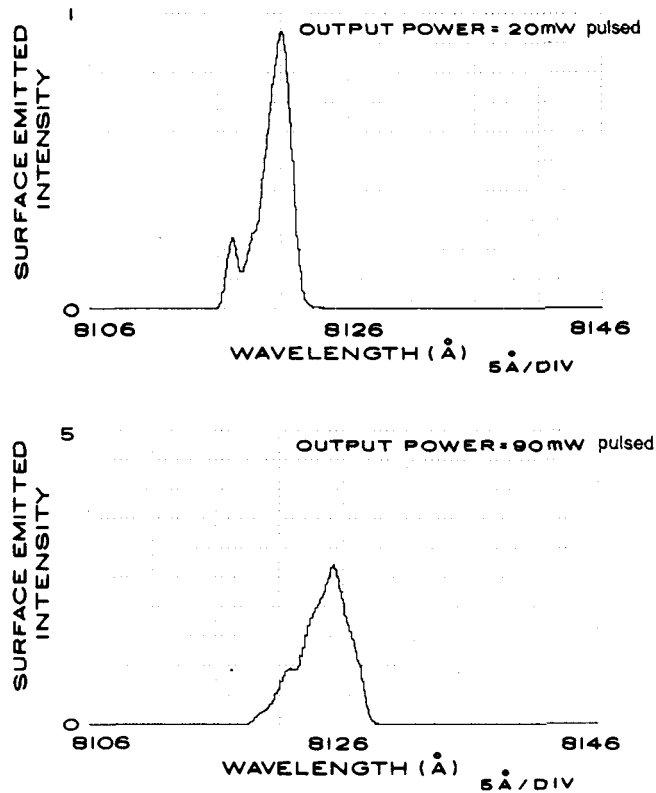
Figure 19. The spectral output for the 1x10 ridge-guided GSE laser array
with a strong grating under pulsed operating conditions.

For a given GRINSCH structure, the strength of the grating coupling in the
DBR sections is determined by the depth of the grating and the thickness of the
remaining p-cladding in the DBR section. This can be understood by considering
the diagram in Fig. 20, where the shape of the transverse mode is shown in the
DBR section. The grating coupling coefficient is proportional to the overlap of the
guided mode profile with the grating layer. Therefore, the deeper the grating or
the closer the grating layer is to the guide layer (provided enough cladding
remains so that the mode remains guided) the stronger the interaction between
the guided mode and the grating. This stronger interaction could give rise to an
increase in reflectivity and a decrease in transmissivity, which would lower the
power output. Since there is still no universally accepted model for calculating
the reflectivity, transmissivity, and output coupling properties of second order
DBR waveguides, it is not yet possible to accurately quantify the relationship
between the grating parameters and the mode coupling. In Fig. 20 the mode
overlap with the grating layer is plotted as a function of the range of grating

depths that were used for the 1 x 10 GSE arrays. This type of variation in grating depth gave rise to the different PI characteristics that were shown in the devices discussed above.
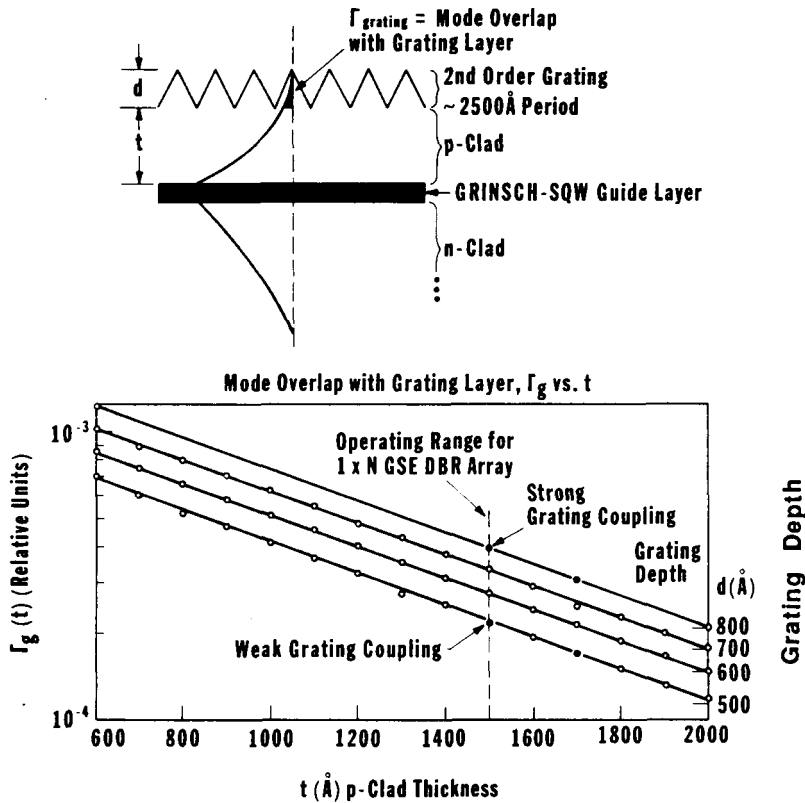
Figure 20. The grating confinement factor is plotted as a function of p-clad thickness along the lower axis for grating depths of 500 Å, 600 Å, 700 Å, and 800 Å. The diagram at the top illustrates the overlap of the guided mode with the grating at the top of the p-clad.

Both the power output and the spectral outputs of the 1x10 GSE arrays clearly fell short of the goals of this program. It was decided that larger arrays would be needed to obtain the higher power outputs required. Also, all facets could be eliminated and more DBR sections would be added to improve the frequency selectivity of the feedback to the gain sections. Since existing 10 x 10 GSE arrays had shown power outputs and spectral outputs that were much closer to the goals of this program, it was decided to use this type of array structure as the baseline design. Also several types of 10 x 10 GSE arrays, that had been developed on earlier programs, were available for investigating the switching and

31

modulation properties of GSE lasers. Modulation of high-power diode laser arrays has not really been explored in either edge-emitters or surface-emitting laser arrays. For communications applications this is a critical issue. Therefore, experiments were planned to develop an efficient method for modulating GSE laser arrays.

E.   10 X 10 TWO-DIMENSIONAL GSE LASER ARRAYS

Monolithic GSE diode laser arrays[14-17] are very attractive devices for potential use in optical communications systems. Compared to conventional edge-emitting diode laser arrays, GSE laser arrays offer many advantages that should lead to superior performance in optical communications systems applications. In a GSE array, the DBR sections couple the gain sections together in such a way that they can all be operated at a single frequency. This occurs because the grating provides frequency selective feedback and optical coupling to the gain sections of the array. In addition, the grating also acts as a large-area output coupler. The advantages over edge emitting arrays are: 1) there are no cleaved facets as in edge-emitting arrays, and thus the problem of facet damage, that can occur at high output powers, is eliminated in GSE laser arrays; 2) the emitting area of the array can be designed sufficiently large to produce a very narrow divergence beam in the far field; and 3) the frequency selective feedback provided by the grating should help towards achieving narrow band spectral output. GSE arrays have already demonstrated pulsed power outputs in excess of 1W, near diffraction limited far-field beam divergences of $1° \times 0.01°$[16,17], and single spectral mode outputs at low power (200 mW pulsed) with less than 0.25 Å bandwidth[17] under pulsed operating conditions with 2% duty cycle and 50-ns-wide pulses. It is clear that the extreme aspect ratio (about 100:1) of the far-field emission in this particular geometry might be difficult to accommodate in most spaceflight optical communications systems. A reconfiguration of the array geometry will be required.

A critical requirement for laser array emitters in optical communications systems is that both the far-field pattern and spectral output remain stable under modulation conditions. GSE laser arrays are monolithic optoelectronic integrated curcuits with multiple independent current inputs. These independent electric inputs make it possible to vary the longitudinal spatial distribution of the driving current to the array. Conventional edge-emitting diode lasers that are excited

with an inhomogeneous longitudinal current distribution can be made to operate in a bistable fashion with switching times of about 1 ns.[18-20] Bistable operation of single gain element GSE lasers with quantum well active layers has now been demonstrated with switching times of about 20 ps.[21] By using such an approach with a GSE array, it may be possible to switch the array rapidly between two stable operating levels at modulation rates high enough for a two-level amplitude-shift-key communications system. In addition, the bistable characteristics of the GSE array should find applications in optical computing and other optoelectronic integrated circuit designs.

To assess the potential of GSE technology for optical communications, experimental studies on the modulation properties of existing one and two dimensional GSE arrays were performed in this phase of the program. In the course of these studies, bistable operation and electro-optic amplification by an injection-coupled GSE semiconductor diode laser array were demonstrated.

F.   10 X 10 TWO-DIMENSIONAL GSE LASER ARRAYS WITH Y-COUPLED GAIN SECTIONS

The first structure investigated, shown in Fig. 21, was a 9 x 10 two-dimensional GSE array with Y-coupled ridge guides in the gain sections. The insets in Fig. 21 show the details of this structure. This array had 9 electrically independent gain sections, each consisting of 10 Y-coupled ridge-guided lasers, that were 150 μm long alternating with 300-μm-long passive DBR waveguide sections. The grating period was such that the laser wavelength was about 70 Å shorter in wavelength than the peak of the spontaneous emission profile. When the laser wavelength is closer to the bandgap, the optical losses due to absorption are greater than for wavelengths that are longer than the peak of the spontaneous emission profile. Therefore, the effect of the saturable loss in a gain section can be tailored sufficiently large to Q-switch the entire array. In Fig. 22 the power vs current (PI) characteristics of the array are shown. Since the array was tested p-side up, low duty cycle 150-ns-long pulses were used to drive the array to minimize heating effects. To obtain the PI curves in Fig. 22, the current pulses to all but the center gain section were maintained at a constant level. The various levels used are indicated next to the right of each curve in Fig. 22 The amplitude of the current pulse to the center gain section was varied (x-axis in Fig. 22) and the power output of the entire array (y-axis in Fig. 22) was measured. As the current to this gain section was varied, the optical output power of the laser

was observed to have a discontinuous turn-on. At this turn-on, an increase in the input current of about 50 mA switched the array optical power output of the array from 40 mW of incoherent power to over 400 mW of optical power (laser oscillation of array). This corresponds to an effective differential efficiency of over 400%. The discontinuous nature of this transition is shown in Fig. 23. When the current to the center gain section was tuned near the center of the steep part of the PI curve (as shown by the inset in Fig. 23) the time-resolved output (as detected by a PIN diode with 20 ns rise time) was a superposition of two distinct pulse shapes, designated as on-state (lasing condition) and off-state (non-lasing condition) in Fig. 23. The appearance of such distinct pulses with constant amplitudes throughout the steep transition region of the PI curve indicates bistable switching. For stable operation (no bistable switching), a continuous variation in the amplitude of optical pulse output would have been observed as the injection current was tuned through the steep transition region of the PI curve. Similarly for unstable operation, a continuum of pulse amplitudes would have been observed simultaneously in the steep transition region of the PI curve. As the current to the center gain section was tuned through the transition to higher current values, the off-state pulse disappeared and only the on-state remained. Conversely, as the current was tuned through the transition to lower currents, the on-state pulse disappeared leaving only the off-state pulse. The simultaneous observation of the two output pulses over the narrow current range that corresponded to the transition in the PI curve indicates bistable switching. It is seen that the array output switches very rapidly between the on and off states. This bistable behavior is only observed within about a 30 mA to 50 mA current range that defines the transition region of the PI curve. The PI switching characteristics of this array are very much like those of a transistor. The series resistance of the array was estimated to be about 10 Ω. Therefore, an increase of the electric power into the array by only about 25 mW produced an increase in the optical power output of around 400 mW, corresponding to a electro-optic power gain of 12 dB. This was the first demonstration that a GSE laser array can operate in a bistable manner and also function as an optical amplifier of electrical pulses.

N = # of Injection-Coupled Gain Sections

M = # of Laterally-Coupled Lasers per Gain Section

Y-Ridge Guided Gain Section

2μm

5μm

p-Clad ~0.1μm
Active
n-Clad

GRINSCH-SQW Active Layer

Mole Fracture AlAs

100
80
60
40
20
0

Cap (0.2μm)

p-Clad
(1.2μm)

n-Clad
(1.2μm)

Graded
Regions
(0.4μm)

Substrate

Quantum Well (50Å)

N x 10 GSE

300μm

150μm

2nd Order Grating

~2500Å Period

al_{in}

l_{in}

rl_{in}

tl_{in}

p-Clad ~0.1μm
Guide Layer
n-Clad

2nd Order DBR Passive Waveguide Section

Figure 21. A schematic diagram of a monolithic two-dimensional 10 x 10 GSE diode laser array with 10 Y-coupled lasers in the gain sections. The insets show the geometry of the Y-coupled ridge-guide lasers in the gain sections, the structure of the GRINSCH-SQW active/waveguide layer, and the DBR passive waveguide structure.
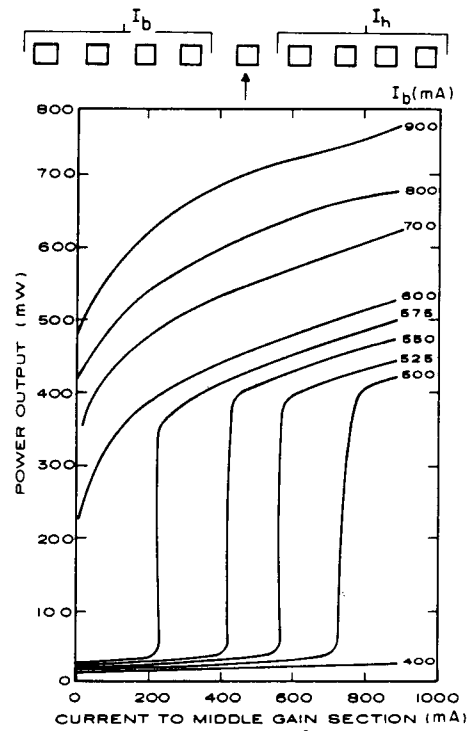
Figure 22. Optical power output vs current to the center gain section of a 9 x 10 GSE array. A region of bistable operation is clearly seen.
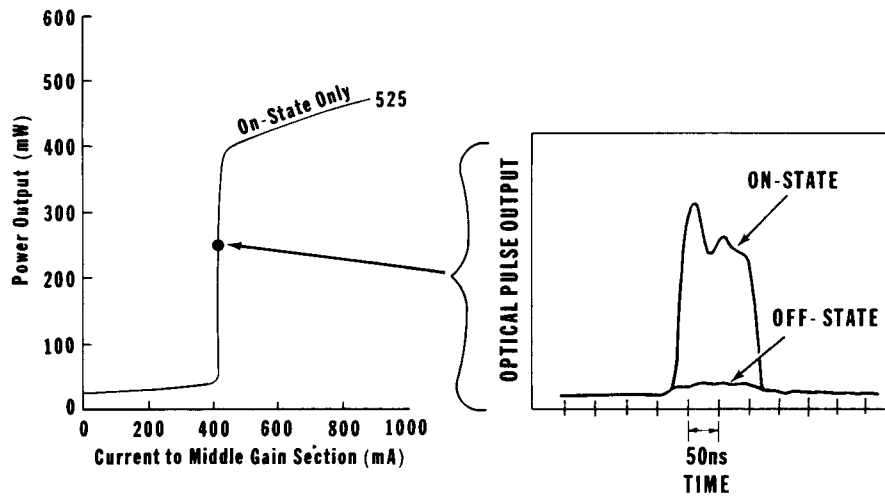
Figure 23. Oscilloscope trace of the optical pulse output of the 9 x 10 GSE array when it was operated in the center of the switching region (shown in PI curve on left).

35

In order to demonstrate modulated operation of a GSE array, a prototype high-frequency mount was designed so that the high speed characteristics of this switching behavior could be studied in more detail. Arrays with bistable characteristics were identified by probe testing for subsequent sawing from the wafer and mounting in a high frequency mount. The mounted array, shown in Fig. 24, was operated in a pulsed mode with no dc bias and the light output was detected using a Si avalanche photodiode detector. Measurements of the rise time of the optical pulse of a mounted array are shown in Fig. 25. The current pulse to the center array element is shown in Fig. 25a, and the resulting optical output pulse is shown in Fig. 25b. The optical pulse has a rise time of only 420 ps, considerably less than that of the current pulse. This occurs because the switching effect due to the saturable loss has a much faster time constant than the current pulse. The ripple on top of the pulse is probably due to a slight impedance mismatch in the cable connection between the detector and the oscilloscope. The time-averaged far field of the array and the corresponding spectral output is shown in Fig. 26. This spectrum was obtained with an optical spectrum analyzer that has a resolution of about 1 Å. Even though the output of this array has temporal features as short as 420 ps, the spectral bandwidth is about 1 Å at 3 dB down and broadens to 2 Å at 15 dB down, with 30 dB side-mode rejection. This broadening is probably due to frequency chirp or longitudinal mode hopping due to the severe modulation conditions (i.e., p-side mounting, 50 ns pulses, and no dc bias). Also, the time-averaged far field shows a well-resolved dominant single lobe. This is an indication that the far-field is stable under the bistable switching. This is to be expected for this type of modulation where the laser array is switched between two discrete states. Far-field instabilities would be more likely to occur in lasers that are switched through a continuum of operating levels. While higher speed measurements and narrower spectral resolutions must still be done this result shows the potential for switching at data rates of several hundred MHz with 1-3 Angstrom wavelength chirp and a time averaged stable far-field output.

Switching input

GSE array

Bias inputs

1 2 3 4 5 6 7 8
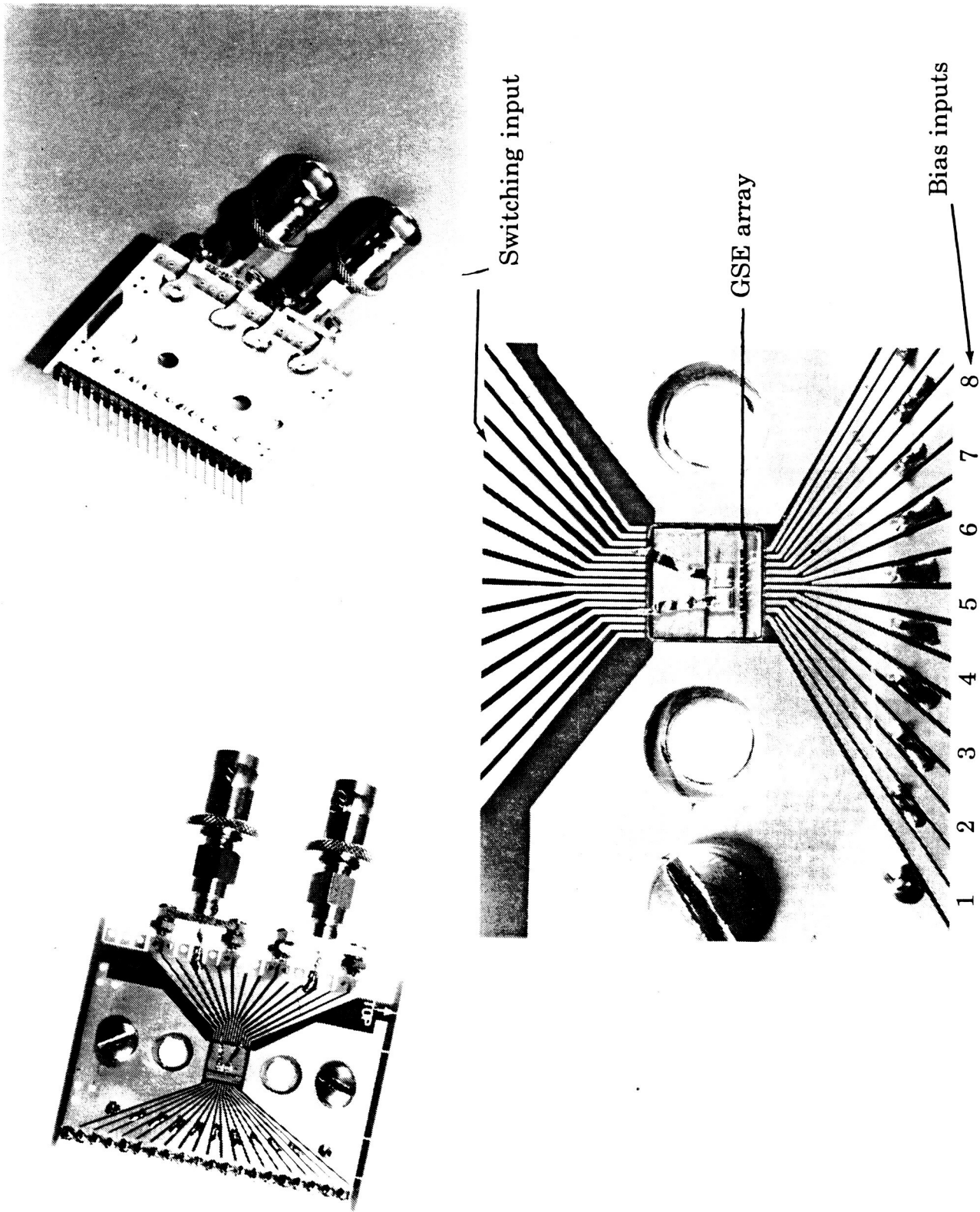
Figure 24. Photographs of a prototype high-speed mount for modulating GSE arrays.

Current Pulse

(a)

Current Amplitude

|← 10ns →|

Light Pulse

(b)

Optical Intensity

|← 420ps →| |← 1ns →|

Relative Time
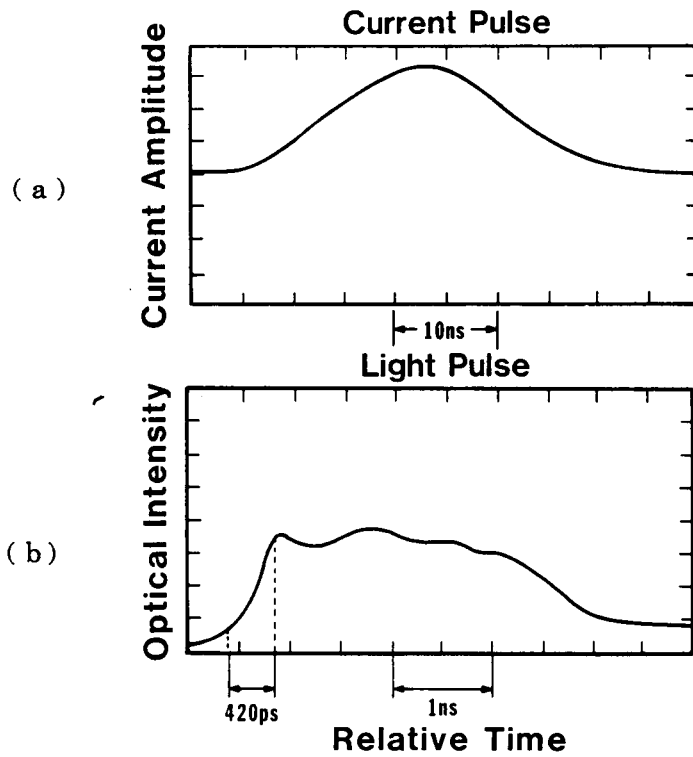
Figure 25. a) Short pulse output of a bistable GSE array showing 420 ps
rise time and b) the wavelength spectrum of these pulses.

-40

dB

1.2°   -60

-80
0.8474   0.8484   0.8494
Time-Averaged Far-Field Output   Res 0.1nm   0.2nm/div

Spectral Output

(a)   (b)
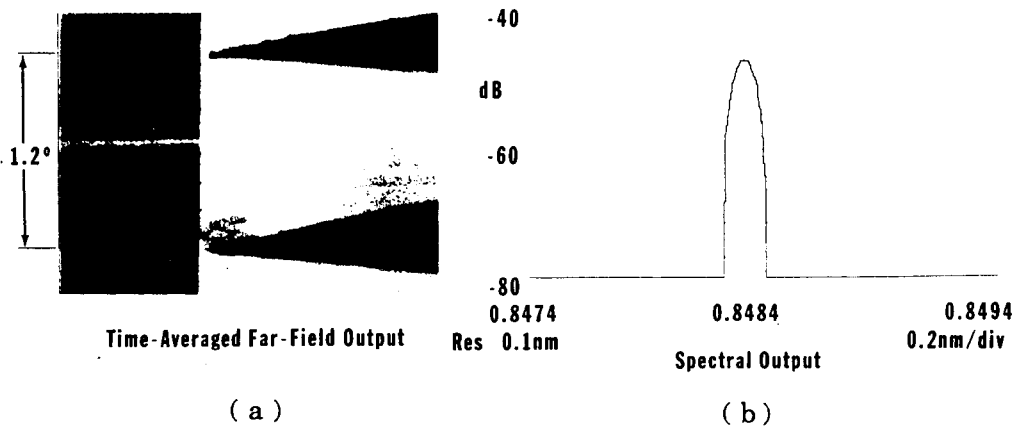
Figure 26. a) Far-field output and b) spectrum of the optical pulse output
(pulse form shown in Fig. 25) of the 6x10 GSE array.

The bistable switching effect described above could prove to be a very efficient technique for amplitude modulation of GSE laser arrays. In Fig. 27, a schematic diagram shows how a bistable GSE array might be operated as a high speed digital transmitter. The array is biased just below the steep slope of the power current curve. A capacitively coupled radio-frequency pulse is used to drive only the center gain section so that the entire array can be switched on and off as it is driven through the sharp transition region of the power-current curve.
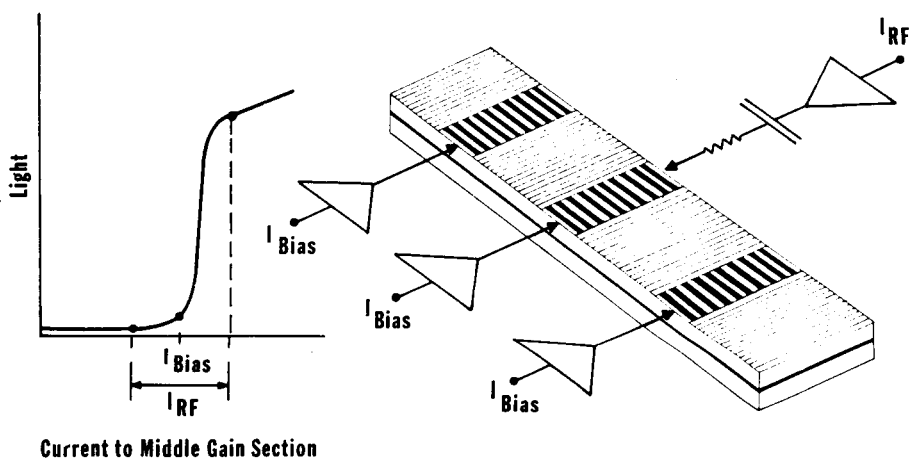
Figure 27. Diagram showing how a GSE array might be modulated by switching between the on and off states associated with the bistable transition using rf pulses.

Another 10x10 GSE array that was found to exhibit bistable switching behavior under probe testing was also mounted so that it could be tested under burst modulated operating conditions. After the array had been bonded, it no longer exhibited the abrupt bistable switching characteristic in the PI curve. However, the array did demonstrate wavelength switching and far-field beam steering. Under pulsed operating conditions with 100 ns pulses to all gain sections, the operating wavelength of this array could be switched 140 Å by changing the current to the sixth gain section by about 30 mA. Each operating wavelength corresponded to a different far-field pattern as shown in Fig. 28a and 28b. When an rf current was used to drive the sixth gain section and long (100 ns) pulses drove the remaining gain sections, the resulting time-averaged far-field pattern appeared as a superposition of the two far fields shown in Fig. 28a and 28b. This is illustrated in Fig. 28c and 28d, where rf pulses of 320 MHz and 2.4 GHz, respectively, were applied to the sixth gain section. Similar results were obtained for rf pulses with other frequencies. In Fig. 29, the spectral

output of the far-field output of the array under modulation is shown. Fig. 29a is the spectrum of only the center lobe of the far field, while Fig. 29b is the spectrum of the lobes that are separated by about ±3° from the center lobe. The angular differences of the far fields are consistent with the wavelength difference. The predominantly single-lobed on-axis far field corresponds to the wavelength at around 8500 Å, and is due to laser oscillation caused by the DBRs. The far field that is comprised of the two lobes that are separated by about 6° corresponds to the wavelength range from 8640 Å to 8645 Å. Laser oscillation at these wavelengths is very likely caused by one or both of the facets on the terminating DBR sections this array. More experiments will be necessary in order to develop a complete understanding of this wavelength switching phenomena. Although, the power requirements and spectral stability of this source need to be improved, the high-speed beam steering could possibly be exploited as a technique for modulating GSE arrays.

This high-speed wavelength switching and beam steering phenomena could possibly be used in a two level amplitude shift keying (ASK) communications system. A detector that subtended a solid angle equal to or less than that of the central lobe could be placed along the 0° axis in the far field. A multi-Gbit ASK communications link would be obtained by using the high-speed beam steering effect described above to steer the far-field output of the transmitter beam on and off of the receiver in the far field. Using large angle beam steering as a technique for amplitude modulation could lead to lower bit-error-rates than in conventional ASK systems, since a larger dynamic range between the on and off levels may be possible using beam-steering amplitude modulation.

. The experimental investigations of switching and modulation properties of GSE arrays have uncovered some unique properties of these devices. The methods found for modulating GSE laser arrays offer potential advantages over more conventional techniques. With improvements in designs that are aimed at improving spatial and spectral mode stability under dynamic operating conditions, it is anticipated that a GSE laser transmitter can be developed. These design improvements and these implementation are described in the next section.
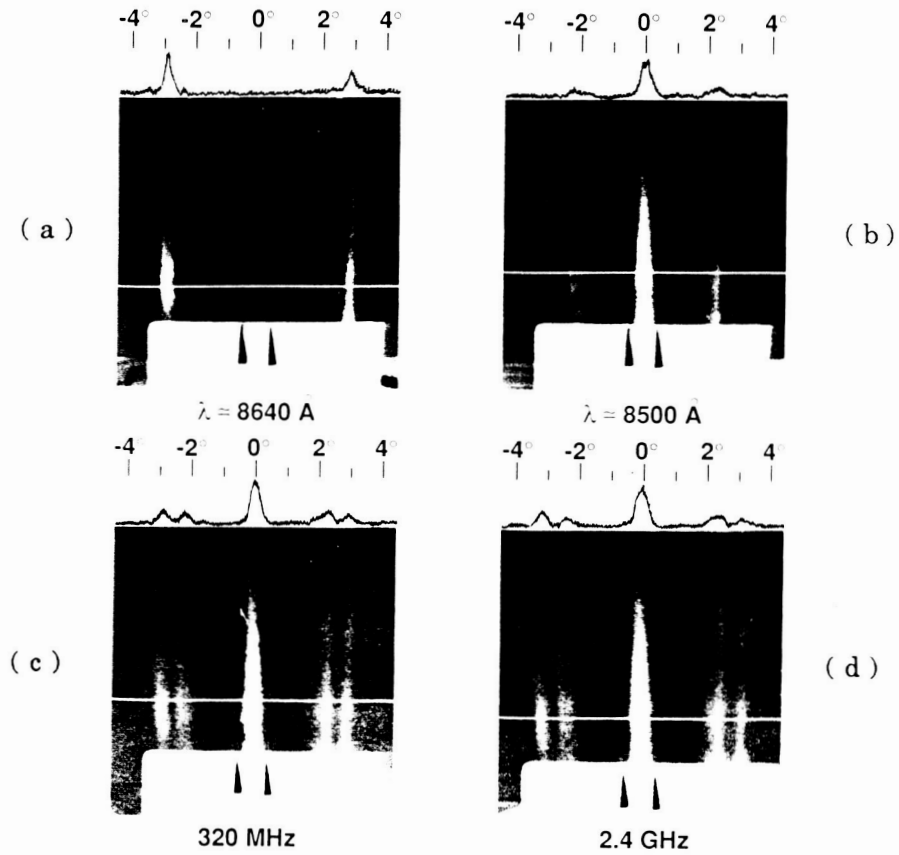
Figure 28. a) The time-averaged far field output of a 10 x 10 GSE array is shown operated at 8640 Å and b) 8500 Å. c) Using radio-frequency pulses of 320 MHz and d) 2.4 GHz to drive one gain section of the array produced a superposition of the far-fields that were observed at 8640 Å and 8500Å.
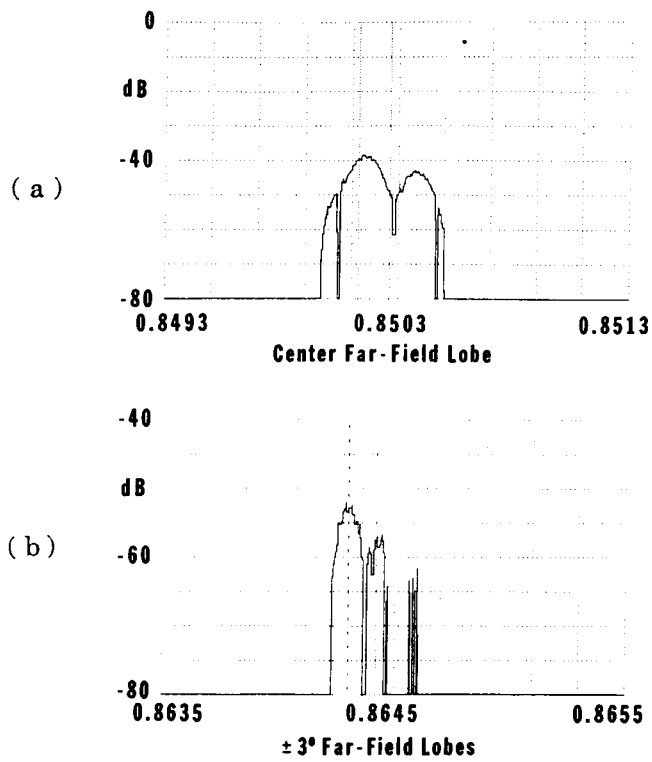
Figure 29. Spatially resolved spectra of the center far field lobe shown in Fig. 28 a) and the far-field lobes at 3° off axis in Fig. 28 b) show operation at wavelengths of 8640 Å and 8503 Å.

43

Section V

CONCLUSION

The development of practical, reliable phased-array sources is a high risk, high payoff venture that has been considerably advanced by the development of GSE technology over the past three years. The problems of realizing the potential of this source for optical spaceborne communications are significant, however, and include the following considerations that have not yet been completely addressed in Phase 1 of this program.

- The long-term control of multiple current sources to maintain injection coupling in large GSE arrays

- The development of an optimized geometry of two-dimensional surface emitters that will allow propagation of a circular cross-section beam from the transmitting telescope

- The demonstration of sufficiently stable operation over the required systems lifetime to make GSE devices useful components for space communications links

The first two considerations are primarily systems issues that cannot reasonably be addressed completely at the present time without knowledge of the ultimate capabilities and limitations of the GSE technology. We can conceive of partial solutions now, however, and our best engineering judgement is that these considerations, by themselves, are not as significant risks to the development of a useful source as is the design and fabrication of the surface-emitting arrays themselves. The issue of operating lifetime is, of course, still open and ultimately extremely critical. An inherent advantage of the GSE concept is, however, that many emitters can be coupled, thus reducing the requirements for individual emitter performance. This is important because no individual, diffraction-limited edge-emitting source has demonstrated adequately long performance at even 100 mW cw without degradation. It may well be possible to reduce the output requirements of each emitter of a GSE array to very modest levels, for which long life, even in AlGaAs, can be demonstrated. In addition, the large emitting area of the grating in such a device reduces the light flux considerably (two orders of

magnitude), so that the non-radiative recombination processes that strongly degrade edge-emitting AlGaAs lasers can be effectively eliminated.

In summary, we have outlined an approach to continuing the development of the GSE device for optical communications. We believe this device has already demonstrated the potential for attaining the source needs required, but will require further development to optimize the design and fabrication processes necessary to achieve the full performance and reliability demanded of components in practical spaceborne systems.

Section VI

REFERENCES

1. J. K. Butler, D. E. Ackley, D. Botez, "Coupled-mode analysis of phase-locked injection laser arrays," Appl. Phys. Lett. 44, 293, (1984).

2. R. Smith, "Calculation of Complex Propagating Modes in Arbitrary, Plane-Layered, Complex Dielectric Structures", Ph. D. Thesis, Univ. of Washington, 1978.

3. A. Yariv, "Coupled-Mode Theory for Guided-Wave Optics", IEEE J. Quantum Electron. QE-9,729,(1975).

4. N. S. Kapany and J. J. Burke, "Optical Waveguides," Academic Press, New York, 1972.

5. E. Kapon, J. Katz, A. Yariv, "Supermode analysis of phase-locked arrays of semiconductor lasers," Opt. Lett. 10, 125 (1984).

6. B. Goldstein, N. W. Carlson, G. A. Evans, N. A. Dinkel, V. J. Masin, "Performance of a channelled-substrate-planar high-power phase-locked array operating in the diffraction limited," Electon. Lett. 23, 1136, (1987).

7. N. W. Carlson, V. J. Masin, M. Lurie, B. Goldstein, G. A. Evans, "Measurement of the coherence of a single-mode phase-locked diode laser array," Appl. Phys. Lett. 51, 643, (1987).

8. L. J. Mawst, D. Botez, T. J. Roth, G. Peterson, J. J. Yang, "Diffraction-coupled, phase-locked arrays of anti-guided, quantum-well lasers grown by metalorganic chemical vapor deposition," Electron. Lett. 24, 958, (1988).

9. D. Botez, L. J. Mawst, G. Peterson, "Resonant leaky-wave coupling in linear arrays of anti-guides," Electron. Lett. 24, 1328, (1988).

10. D. Marcuse, "Theory of Dielectric Optical Waveguides," Academic Press, New York, 1974.

11. J. K. Butler, G. A. Evans, N. W. Carlson,"Nonlinear Characterization of Modal Gain and Effective Index Saturation Channelled-Substrate-Planar Double-Heterostructure Lasers", IEEE J. Quantum Electron. 25, 1646, (1989).

12. B. Goldstein, M. Ettenberg, N. A. Dinkel, J. K. Butler, "A high-power channelled-substrate-planar AlGaAs laser, Appl. Phys. Lett. 47, 655, (1985).

13. N. W. Carlson, "Coherent High-Power Phase Array Laser Semiconductor (CHIPPALS) ,", ASD/PMREA Contractor Report F33615-85-C-1858, May 1989.

14. N. W. Carlson, G. A. Evans, J. M. Hammer, M. Lurie, S. L. Palfrey, M. Ettenberg, L. A. Carr, F. Z. Hawrylo, E. A. James, C. J. Kaiser, J. B. Kirk, W. F. Riechert, J. R. Shealy, J. W. Sprague, S. R. Chinn, P. S. Zory, "Dynamically stable 0° phase mode operation of a grating-surface-emitting diode -laser array," Opt. Lett. 13, 312, (1988).

15. N. W. Carlson, G. A. Evans, J. M. Hammer, M. Lurie, L. A. Carr, F. Z. Hawrylo, E. A. James, C. J. Kaiser, J. B. Kirk, W. F. Riechert, D. A. Truxal, J. R. Shealy, S. R. Chinn, P. S. Zory, "High-power operation of a grating-surface-emitting diode -laser array with 0.012° far-field angle," Appl. Phys. Lett. 52, 939, (1988).

16. G. A. Evans, N. W. Carlson, J. M. Hammer, M. Lurie, J. K. Butler, S. L. Palfrey, R. Amantea, L. A. Carr, F. Z. Hawrylo, E. A. James, C. J. Kaiser, J. B. Kirk, W. F. Riechert, J. R. Shealy, S. R. Chinn, P. S. Zory, "Coherent, monolithic two-dimensional (10x10) laser arrays using grating surface emission," Appl. Phys. Lett. 53, 2123, (1988).

17. G. A. Evans, N. W. Carlson, J. M. Hammer, M. Lurie, J. K. Butler, S. L. Palfrey, R. Amantea, L. A. Carr, F. Z. Hawrylo, E. A. James, C. J. Kaiser, J. B. Kirk, W. F. Reichert, "Two Dimensional Coherent Laser Arrays Using Grating Surface Emission", IEEE J. Quantum Electron. 25, 1525, (1989).

18. J. K. Carney, C. G. Fonstad, "Double-heterostructure Laser Diodes with Multiply Segmented Contacts", Appl. Phys. Lett. 38, 303,(1981).

19. H. Kawaguchi, "Optical Bistable-Switching Operation in Semiconductor Lasers with Inhomogeneous Excitation", IEEE Proc. Vol. 141, 141, (1982).

20. Y. Arakawa, A. Larson, J. Paslaski, A. Yariv, "Active Q-switching in a GaAs/AlGaAs multiquantum well laser with an Intracavity Monolithic Loss Modulator", Appl. Phys. Lett. 48, 561, (1986).

21. R. Amantea, S. L. Palfrey, N. W. Carlson, "Network model for two-dimensional coupled laser arrays," Opt. Lett. 14, 30 (1989).

22. N. W. Carlson, G. A. Evans, R. Amantea, S. L. Palfrey, J. M. Hammer, M. Lurie, L. A. Carr, F. Z. Hawrylo, E. A. James, C. J. Kaiser, J. B. Kirk, W. F. Riechert,"Performance characteristics of coherent two dimensional grating surface emitting diode laser arrays," IEEE Lasers and Electro-Optics Society 1988 LEOS Annual Meeting, Conference Proceedings, 444, (1988).

Report Documentation Page

1. Report No. NASA CR-181869	2. Government Accession No.	3. Recipient's Catalog No.

4. Title and Subtitle		5. Report Date
AlGaAs Phased Array Laser for Optical Communications		September 1989
		6. Performing Organization Code

7. Author(s)	8. Performing Organization Report No.
N. W. Carlson	
	10. Work Unit No. 506-44-21-01

9. Performing Organization Name and Address	11. Contract or Grant No.
David Sarnoff Research Center CN 5300 Princeton, NJ 08543-5300	NAS1-18525
	13. Type of Report and Period Covered

12. Sponsoring Agency Name and Address	Final Report 8/6/87 - 6/9/89
National Aeronautics and Space Administration Langley Research Center Hampton, VA 23665-5225	14. Sponsoring Agency Code

15. Supplementary Notes

Langley Technical Monitor: Herbert D. Hendricks

16. Abstract

Phased-locked arrays of multiple AlGaAs diode laser emitters have been investigated both in edge-emitting and surface-emitting configurations. CSP edge-emitter structures, coupled by either evanescent waves or Y-guides, could not achieve the required powers ($\geq$ 500 mW) while maintaining a diffraction-limited, single-lobed output beam. Indeed, although the diffraction limit was achieved in this type of device, it was at low powers and in the double-lobed radiation pattern characteristic of out-of-phase coupling. Grating-surface-emitting (GSE) arrays were, therefore, investigated with more promising results. The incorporation of second-order gratings in distribute Bragg reflector (DBR) structures allows surface emission, and can be configured to allow injection-locking and lateral coupling to populate two-dimensional arrays that should be able to reach power levels commensurate with the needs of high-performance, free-space optical communications levels. Also, a new amplitude modulation scheme was developed for GSE array operation.

17. Key Words (Suggested by Author(s))	18. Distribution Statement
Phased-arrays, grating-surface-emitters, amplitude modulation	Unclassified - Unlimited Subject Category 36

19. Security Classif. (of this report)	20. Security Classif. (of this page)	21. No. of pages	22. Price
Unclassified	Unclassified	49	